Atmos. Chem. Phys., 5, 2635–2656, 2005
www.atmos-chem-phys.org/acp/5/2635/
SRef-ID: 1680-7324/acp/2005-5-2635
European Geosciences Union

Atmospheric Chemistry and Physics

Two decades of OH variability as inferred by an inversion of atmospheric transport and chemistry of methyl chloroform

P. Bousquet[1,2], **D. A. Hauglustaine**[1], **P. Peylin**[1,3], **C. Carouge**[1], **and P. Ciais**[1]

[1]Laboratoire des Sciences du Climat et de l'Environnement (LSCE), Gif sur Yvette, France
[2]Université de Versailles Saint Quentin en Yvelines (UVSQ), Versailles, France
[3]Laboratoire de Biogéochimie des milieux continentaux, UMR INRA-CNRS-PARIS 6, INRA-INAPG, Thiverval-Grignon, France

Received: 23 December 2004 – Published in Atmos. Chem. Phys. Discuss.: 18 March 2005
Revised: 13 June 2005 – Accepted: 6 September 2005 – Published: 4 October 2005

Abstract. We developed an iterative inverse method to infer inter-annual sources and sinks of methyl chloroform (MCF) from atmospheric measurements, on a monthly basis. The methodology is presented and used to estimate two decades of OH variability between 1980 and 2000, using varying meteorology. When OH concentrations are adjusted with loose prior errors and MCF emissions are adjusted within inventory bounds, we show that substantial OH inter-annual variability (8.5±1.0% of the mean) and trend ($-0.7\%.\mathrm{yr}^{-1}$) are necessary to match MCF observations. This result is confirmed by a series of sensitivity tests addressing main limitations of previous studies. However, we show that it is also possible to match MCF observations with a 65% reduction of OH year-to-year variations and a 60% reduction of absolute OH trend, but still a consistency of inferred emissions with inventory values at a $\pm 2\sigma$ level. On the other hand, the phase of inferred OH variations is a more robust feature of our set of inversions. Overall, MCF inversions can only provide a range of OH variations unless inventory uncertainties are further reduced.

1 Introduction

Hydroxyl radical (OH) is the main oxidant of the atmosphere as it reacts with most pollutants including methane (CH4), carbon monoxide (CO), Non-Methane Hydrocarbons, and halogenated species, such as 1,1,1-trichloro-ethane (CH_3CCl_3, methyl-chloroform, hereafter referred as MCF). The production of OH radical in the troposphere is due to the reaction of excited atomic oxygen (O^{1D}) produced by the photolysis of ozone (λ<320 nm) with water vapor. At a global scale, mean OH concentration is estimated to be around 10.10^5 molecules.cm^{-3}, ranging from 8.10^5 cm^{-3} to 12.10^5 cm^{-3} (IPCC, 2001), with large spatial, diurnal and seasonal variations depending mainly on available radiation, ozone content and water vapor concentrations (Spivakovsky et al., 2000). As OH plays a major role in the removal of trace gases in the troposphere, quantifying year-to-year to decadal changes of chemically active species, such as methane, requires a good knowledge of OH OH space and time variations. The very short residence time of OH in the troposphere makes it difficult to get OH variability at regional to global scales. Thus, proxy methods were proposed to estimate its variability. One can use a trace gas with known and simple sources that reacts with OH radical. Methyl Chloroform has already been employed by several authors to infer OH fields based on different methodologies (Krol et al., 2003; Dentener et al., 2002; Prinn et al., 1995, 2001; Houweling et al., 1999; Hein et al., 1997).

Since 1978, MCF has been measured at five stations over the world by ALE/GAGE/AGAGE programs (Prinn et al., 2000). More recently, since the early 1990s, NOAA/CMDL has measured MCF at 10 remote locations (Montzka et al., 2000). MCF is mainly removed from the atmosphere by its reaction with hydroxyl radical (OH) with a lifetime estimated to be around 5 years (Prinn et al., 2001; Montzka et al., 2000; WMO, 2002). So far, ALE/GAGE/AGAGE atmospheric measurements of MCF have been widely used to scale global and hemispheric OH distributions in the troposphere. Hein et al. (1997) and Houweling et al. (1999) have used MCF measurements in the atmosphere to adjust globally their OH field before optimizing time-averaged CH_4 sources with a chemical transport model (CTM). More recently, year-to-year variations of OH have been optimized against MCF measurements through inverse procedures based on two-dimensional zonal CTM (Prinn et al., 2001) and 3-D-CTM (Krol et al., 2003) with climatological meteorology and transport. In these studies, yearly scaling factors of OH field were inferred at a global scale for each year over the period 1978–2000. Both studies found a large increase in the global OH

Correspondence to: P. Bousquet
(pbousquet@cea.fr)

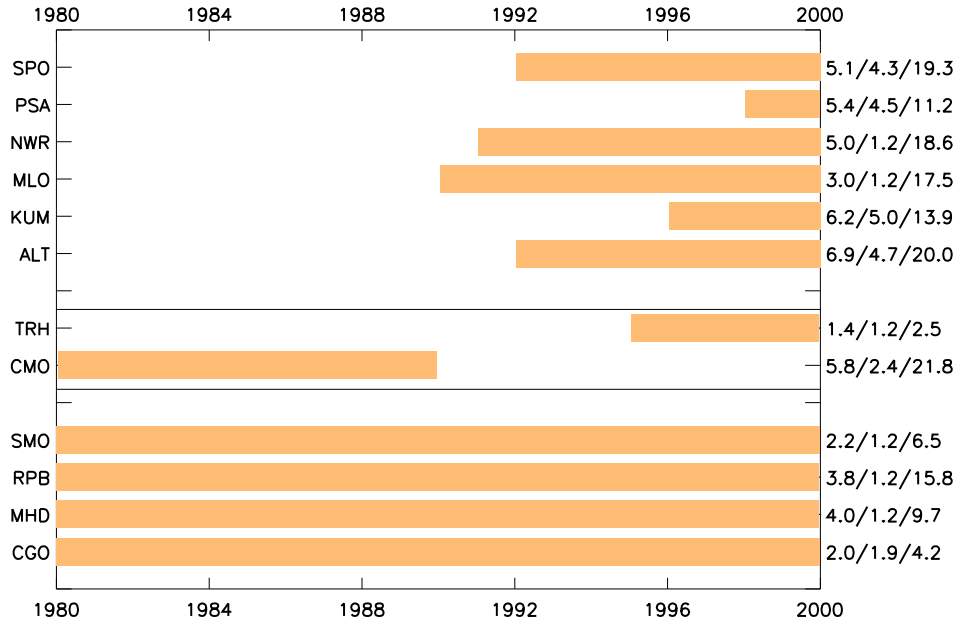

Fig. 1. Observation timeframe and uncertainties used for inversions. Grey bars figure the period for which we have observations at each station. For each station, groups of three numbers represent mean uncertainty, minimum uncertainty and maximum uncertainty, respectively (over 1979–2000 period).

abundance during the period 1978–1990 (around +1% yr^{-1}), followed by a large decrease at about the same rate during the following period 1991–2000. They also obtained year-to-year changes in global OH of similar magnitude to the decadal trends (see Fig. 1 of Krol and Lelieveld, 2003, and Fig. 2 of Prinn et al., 2001). However, the two studies disagree in the late 1990s on the amplitude of the decrease, likely due to model differences, and during a period when MCF emissions were very small, producing smaller gradients in the atmosphere that are more difficult to translate in terms of OH variations (Krol et al., 2003).

According to Dentener et al. (2002), variations of OH inferred by those studies on annual and decadal timescales are difficult to reconcile with the observed CH_4 growth rate variability as they would require unrealistic variability of methane sources. Using a 3-D-CTM to quantify the impact of the main factors which control the trend and variability of OH, Dentener et al. (2002) infer a significant but smaller $0.28\pm0.09\%$ yr^{-1} increase in OH during the period 1979–1989, due to a combination of meteorological and chemical effects. Again, in Dentener et al. (2003), year-to-year changes of global OH are of the same order of magnitude as decadal changes, but, both are 3 to 4 times less than the >10% inter-annual variations in OH inferred by Krol et al. (2003) and Prinn et al. (2001). However, in their work, Krol and Lelieveld (2003) argue that such large variations are actually due to modeling errors (inter-annual transport, emissions, too coarse resolution) and that OH can only be optimized on longer timescales only. Thus one faces an apparent inconsistency between CH_4 and MCF budgets as analyzed through OH variability.

Several inverse procedures have been proposed to optimize the sources of chemically active species against atmospheric observations, such as CH_4 and MCF. Dentener et al. (2003) developed a mass balance inversion to analyze inter-annual sources of methane using a 3-D CTM with calculated OH fields. This method has the advantage of accounting for all the non-linearity of atmospheric chemistry but remains rather crude in terms of inversion. For MCF, Prinn et al. (2001) developed a Kalman filter approach but only a 2-D parametrized model was used to simulate transport and chemistry, whereas Krol and Lelieveld. (2003) have implemented a variational inverse scheme based on an iterative minimization of a Bayesian cost function in a 3-D CTM. However these two approaches only optimized one OH scaling factor per year. In particular, they ignored 1. the possibility to optimize seasonal variations of OH field, 2. spatial variations of MCF emissions, and 3. inter-annnual variations of meteorology. Also, in Prinn et al. (2001) the impact of MCF emissions errors on OH variability is estimated using a Monte-Carlo approach but not in Kroll and Lelieveld (2003). Point 2 means that if the prior spatio-temporal variations of MCF emissions and/or of OH fields are incorrect, they cannot be corrected by the inverse procedure. Point 3 has been shown to have a potentially large impact on methane inter-annual variations at surface stations (Warwick et al., 2001). Considering the small number of MCF monitoring sites, it is hopeless to optimize a large number of regions or high

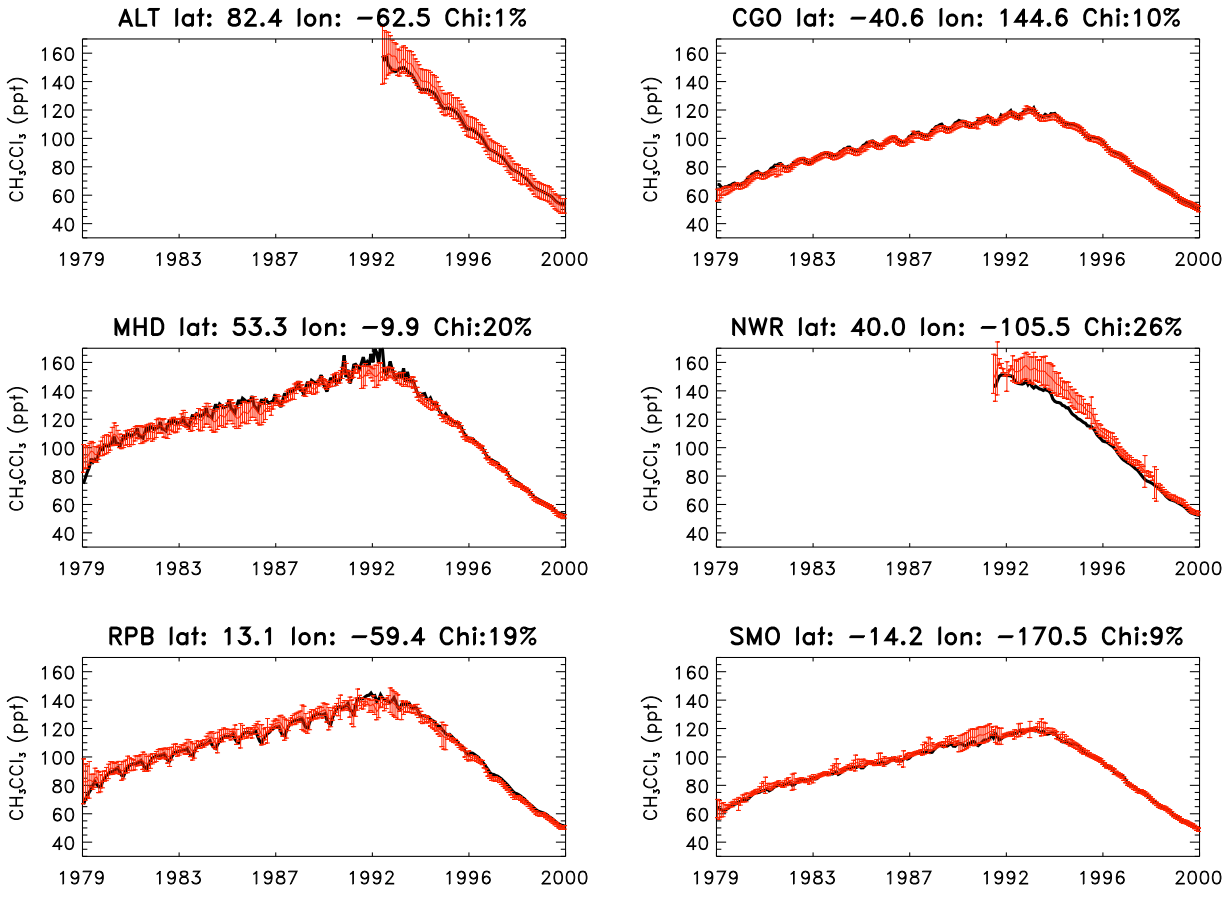

Fig. 2. MCF atmospheric monthly means at 6 stations from 1980 to 2000 (in ppt). Observation and their uncertainties are in red. Optimized model is in black.

frequency OH variations but, as there is at least one station in each large latitudinal band (30°–90° N, 30° N–0°, 0°–30° S, 30° S–90° s) with at least monthly observations, it is reasonable to optimize OH on a monthly basis for these four bands.

In this paper we develop an iterative method to infer chemically active species sources and sinks with long lifetime and apply it to MCF in order to estimate OH year-to-year variations and long-term trend at semi-hemispheric scale for the period 1979–2000. To do so, we perform a Bayesian inversion of MCF measurements, on a monthly basis, using a 3-D Chemistry Transport Model with varying meteorology. The period of inversion is 1979–2000 and the period of analysis is 1980–2000. In the following, we present the inverse procedure (Sect. 2), compare the obtained results with previous studies (Sect. 3) and discuss why large OH variations are inferred and whether these variations are reduced or not when allowing MCF emissions to vary within prior inventory bounds (Sect. 4).

2 Method

Optimizing sources and sinks of a trace gas using a Bayesian inversion requires: 1. atmospheric observations, 2. prior estimates of the sources and sinks distributions, 3. a chemistry-transport model (CTM) to calculate response functions for chemistry and transport, that are the sensitivity of the modeled concentrations to sources and sinks at each station, 4. an inverse procedure, and 5. uncertainties associated to observations and to prior sources and sinks.

A CTM solves the mass conservation equation of the considered gas on a global eulerian grid:

$$\frac{\partial}{\partial t}\left(\rho C_{\mathbf{x},t}\right) = E_{\mathbf{x},t} + T\left(C_{\mathbf{x},t}\right) + \chi\left(C_{\mathbf{x},t}\right), \quad (1)$$

where $C_{x,t}$ represents concentration of the gas at position $\mathbf{x}$ for time t, $E_{x,t}$ stands for its surface sources and sinks, T is the transport operator that can be considered as linear (Enting et al., 1993), and χ represents all chemical processes acting on $C_{\mathbf{x},t}$ (reaction with OH and photolysis for MCF). In the following, we describe a methodology that can be applied to

most long-lived, OH-removed trace gas and we use MCF as a demonstrator of the method.

2.1 Observations

In our standard inversion we use monthly means from 4 stations, Cape-Grim, Tasmania (CGO), Mace-Head, Ireland (MHD), Barbados island (RPB), and Samoa Island (SMO) from the ALE/GAGE/AGAGE network as these are the most consistent long-time series of MCF atmospheric data (Fig. 1). As shown by Rodenbeck et al. (2003), adding or removing stations in an inversion might cause artificial variations. Thus, we did not include Oregon/California (CMO/TRH) data in our standard inversion. We performed two sensitivity tests adding either CMO and TRH stations or 6 stations from the NOAA/CMDL network: Alert (ALT), Kumakahi (KUM), Mauna Loa (MLO), Niwot Ridge (NWR), Palmer Station (PSA), and South Pole (SPO), gradually appearing from 1990, as shown on Fig. 1 (Montzka et al., 2000). All Data have been downloaded from WDCGC Web site (http://gaw.kishou.go.jp/wdcgg.html). No selection was applied to model outputs, whereas a selection procedure is applied by experimentalists (Prinn et al., 2000). In order to test this limitation of our method, we performed a sensitivity test at a northern hemisphere station, using MHD data including pollution events instead of MHD clean-air data. MHD polluted data have been downloaded from AGAGE Web site (http://agage.eas.gatech.edu/).

2.2 MCF surface sources and sinks

MCF is an industrial solvent used in several industrial and commercial processes, such as degreasing of high technology material. MCF emissions ($E_{x,t}$) are given by the Emission Database for Global Atmospheric Research (EDGAR3.2, Olivier et al., 2001). The time evolution of emissions is prescribed for the period 1979–2000, with 1-σ uncertainties from inventory estimates reported by McCulloch and Midgley (2001). Due to a rather long lifetime of 5–6 years (Krol et al., 2003), a significant part of MCF emissions reaches the stratosphere where it contributes to destruction of ozone by releasing active chlorine. Therefore, MCF has been included in the Montreal protocol in 1987 and, its emissions have rapidly and steadily decreased from 1991 ($\sim$718 Gg) to 2000 ($\sim$20 Gg) to reach presently the same level as in the early 1960s ($\leq$20 Gg). Large variations in emissions for the past two decades implied large variations of atmospheric concentrations that peaked at 150 ppt in 1991 in the northern hemisphere (e.g. Mace Head, Ireland) and 120 ppt in 1992 in the southern hemisphere (e.g. Samoa Island), and went down to 40 ppt at present with only a small residual gradient of a few ppt between the northern and the southern hemispheres (Fig. 2 and Prinn et al., 2001).

We accounted for the ocean sink of MCF based on the recent work of Wennberg et al. (2004). Atmospheric MCF transfer to ocean waters is driven by hydrolysis into warm tropical ocean waters and by a higher solubility in cold waters of the mid- and high- latitudes oceans, modulated by the dynamic of ocean-atmosphere interface (Wennberg et al., 2004). Since 1997, MCF has strongly decreased in the atmosphere, and high latitude oceans are found to be a source of MCF for the atmosphere. We divided oceans into 5 zonal regions ($-90°$ S/$-45°$ S, $-45°$ S/$-20°$ S, $-20°$ S/20° N, 20° N/45° N, 45° N/90° N) and used inter-annual estimates from Wennberg et al. (see Fig. 2 of their paper) as prior values for the inverse procedure. In the following, ocean sink is included in the term $E_{x,t}$.

2.3 Transport and chemistry

The transport (T) and Chemistry (χ) terms of Eq. (1) are calculated using the LMDZ-INCA model. LMDZ-INCA is a General Circulation Model (GCM), which includes a chemistry scheme described by Hauglustaine et al. (2004).

The dynamical part of the GCM is based on a finite-difference formulation of the primitive equations solved on a 3-D eulerian grid with a horizontal resolution of 3.75°(longitudes)$\times$2.5°(latitudes) and 19 sigma-pressure layers up to 3 hPa. This corresponds to a vertical resolution of about 300–500 m in the planetary boundary layer (first level at 70 m height) and to a resolution of about 2 km at the tropopause (with 7–9 levels located in the stratosphere). The calculated winds (u,v) are relaxed to ECMWF analyzed meteorology with a relaxation time of 2.5 h (nudging) in order to realistically account for large scale advection (Hourdin and Issartel, 2000). The advection of tracers is calculated based on the finite-volume, second-order scheme proposed by Van Leer (1977) as described by Hourdin and Armengaud (1999). Deep convection is parameterized according to the scheme of Tiedtke (1989) and the turbulent mixing in the planetary boundary layer is based on a local second-order closure formalism (see also Hauglustaine et al., 2004 and Hourdin and Armengaud, 1999). The model has been used recently by Boucher et al. (2002) for the simulation of the sulfur cycle, and by Peylin et al. (2005) and Rivier et al. (2005)[1] for simulations of atmospheric CO_2. The simulated inter-hemispheric exchange time is 1.1 years for fossil CO_2 (Hauglustaine et al., 2004), in the lowest part of the range (1.1–2.1 years) provided by TRANSCOM 1 model inter-comparison (Law et al., 1996; Rayner et al., 1995). This means that LMDZ has one of the fastest inter-hemispheric mixing among the 15 models of TRANSCOM 1. Calculation of source response functions was performed using an offline adjointed version of LMDZ-INCA hereafter called LMDZt, with no chemistry in order to save computational time.

[1] Rivier, L., Peylin, P., Brandt, J., and all AEROCARB project modelers: Comparing Atmospheric Transport Models for Regional Inversions over Europe: Part 2, Estimation of the regional sources and sinks of CO_2 using both regional and global atmospheric models, in preparation, 2005.

Table 1. OH mean concentrations for the four latitudinal bands, for the two hemisphere and at global scale in [$\times 10^5$ cm^{-3}]. Prior values are calculated from MOZART OH field (Hauglustaine et al., 1998). Optimized values come from the mean inversion. Uncertainties are global uncertainties (internal+external, see text). NH/NS ratio is the prior/poste ratio of OH between Northern hemisphere and Southern hemisphere.

OH concentrations	prior	optimized	Prinn et al. (2001)	Krol and Lelieveld (2003)
global	12.1	9.8±0.9	9.4±1.3	10
Northern Hemisphere	13.5	9.0±1.2	8.9±2.0	9.8
30° N–90° N	9.1	6.9±1.4	–	–
0–30° N	17.3	10.7±1.8	–	–
Southern Hemisphere	10.7	10.6±1.4	10.0±2.0	10.2
0–30° S	15.5	14.4±2.1	–	–
30° S–90° S	4.7	6.3±1.5	–	–

For chemistry, we have used a simplified version of LMDZ-INCA including only methyl chloroform chemistry. We consider reaction between MCF and OH:

$$CH_3CCl_3 + OH\bullet \rightarrow CH_2CCl_3\bullet + H_2O \quad \text{(R1)}$$

and photolysis of MCF in the stratosphere:

$$CH_3CCl_3 + h\nu \rightarrow CH_3CCl_2\bullet + Cl\bullet \quad \text{(R2)}$$

OH monthly distribution was pre-calculated by the MOZART CTM (Hauglustaine et al., 1998) and adjusted globally to get a methane chemical lifetime of 8 years within the LMDZ-INCA model. This scaling is however not constraining as we optimize OH concentration in each latitude band. The initial MOZART OH field presents an excess of 25% in the northern hemisphere compared to the southern hemisphere, reflecting a larger photochemical activity in the north. The NH OH excess is in disagreement with estimates from MCF measurements (Montzka et al., 2000) and with Prinn et al. (2001) estimated based on atmospheric modeling but in better agreement with other modeling studies (IPCC, 2001). Table 1 gives the prior OH concentration (mass weighted) for the four latitudinal bands. Only oxidation of MCF by OH radicals and photolysis of MCF in the stratosphere are kept from the original INCA chemical scheme (Hauglustaine et al., 2004).

2.4 Inverse method

The inverse procedure is an evolution of the method of Bousquet et al. (2000) and Peylin et al. (1999) to infer year-to-year changes of CO_2 sources and sinks. New developments include the calculation of inter-annual OH sink response functions, not considered in the case of CO_2. To do so, we have adapted the method of Hein et al. (1997) and Houweling et al. (1999) designed to infer climatological sources and recently used by Wang et al. (2004) to infer methane sources for a reference year (1994). In their approach, reaction with OH is treated separately from emissions, which relies on the linearization of the problem. Transport (T) and chemistry (χ) terms of Eq. (1) can be written:

$$\begin{cases} T\left(C_{\mathbf{x},t}\right) = \nabla.\left(\rho_{\mathbf{x},t} C_{\mathbf{x},t} \mathbf{v}_{\mathbf{x},t}\right) \\ \chi\left(C_{\mathbf{x},t}, [OH]_{\mathbf{x},t}\right) = -k_{\mathbf{x},t}\,[OH]_{\mathbf{x},t}\,C_{\mathbf{x},t} - J_{\mathbf{x},t} C_{\mathbf{x},t} \end{cases} \quad (2)$$

with $k\left(T_{\mathbf{x},t}\right)$ and $J_{\mathbf{x},t}$ representing, respectively, the reaction rates of MCF with OH, and the photolysis rate of MCF. ρ and $\mathbf{v}$ stand for the density and velocity of air. Equation (1) becomes:

$$\frac{\partial}{\partial t}\left(\rho_{\mathbf{x},t} C_{\mathbf{x},t}\right) + \nabla.\left(\rho_{\mathbf{x},t} C_{\mathbf{x},t} \mathbf{v}_{\mathbf{x},t}\right) = E_{\mathbf{x},t} - k_{\mathbf{x},t}\,[OH]_{\mathbf{x},t}\,C_{\mathbf{x},t} - J_{\mathbf{x},t} C_{\mathbf{x},t} \quad (3)$$

As the amount of MCF oxidized by OH or removed by photolysis in a particular location depends on MCF concentration at this location ($C_{\mathbf{x},t}$), MCF concentrations do not respond linearly to MCF emissions. Bayesian inverse formalism can be used for non-linear systems as long as the equations are linearized (Tarantola, 1987) and an iterative procedure is employed (Fig. 3). We thus linearized Eq. (3) around an a priori field of MCF concentration $\hat{C}_{\mathbf{x},t}$:

$$\frac{\partial}{\partial t}\left(\rho_{\mathbf{x},t} C_{\mathbf{x},t}\right) + \nabla.\left(\rho_{\mathbf{x},t} C_{\mathbf{x},t} \mathbf{v}_{\mathbf{x},t}\right) = E_{\mathbf{x},t} - k_{\mathbf{x},t}\,[OH]_{\mathbf{x},t}\,\hat{C}_{\mathbf{x},t} - J_{\mathbf{x},t} \hat{C}_{\mathbf{x},t} \quad (4)$$

We do not optimize the reaction rate, $k_{x,t}$. This is a limitation as Prinn et al. (2001) showed through a Monte Carlo experiment that constant rate was the main contributor to the error in mean OH concentrations. For the first iteration, $\hat{C}_{\mathbf{x},t}$ is obtained running forward the LMDZ-INCA model with an a priori scenario of inter-annnual sources and sinks. A methodology to compute such $\hat{C}_{\mathbf{x},t}$ inter-annual fields at a low numerical cost for the first iteration is given in Appendix A. Surface sources and sinks, $E_{x,t}$, are discretized as monthly pulses for four regions over lands (North America, Europe, Asia, and rest of the world) and 5 zonal regions for oceans (see Sect. 2.2); the OH 3-dimentional sink is discretized as monthly pulses for 4 latitudinal regions (90° S–30° S, 30° S–0°, 0°–30° N, 30° N–90° N), and stratospheric

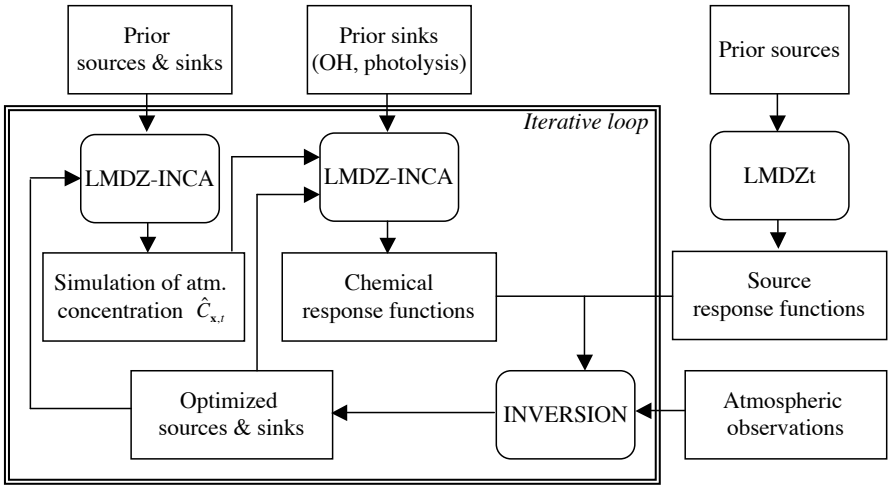

Fig. 3. Flow diagram for inverse procedure. For iteration 1, CTM in run to generate a one-year climatological run (12 months) from which one year of monthly chemical response functions are calculated and then extrapolated over 1979–2000 (Appendix C). Then a first inversion is performed. For iteration 2, CTM is run inter-annually (1979–2000) with varying sources and sinks (from iteration 1), and varying meteorology to generate prior 3-D atmospheric MCF fields that are used as initial conditions to calculate 24 years of monthly chemical response functions. Then a second inversion is performed. Source response functions are calculated once using the adjoint of the CTM together with prior patterns from MCF inventory and varying meteorology (only for 1990–2000).

photochemical loss is only distretized as annual global pulses (the seasonal cycle is small). The integration period is 1979–2000. The response function of a given source/sink $X_{j,m}$ (for region j, and month m or year a) and at a given site i is defined as the partial derivative of the modeled MCF concentrations at station i with respect to $X_{j,m}$. Using the linearized form of Eq. (4), the response functions due to the MCF surface sources and sinks ($\tilde{C}_{E_{j,m},i}$), the OH sink ($\tilde{C}_{OH_{j,m},i}$) and the photochemical loss ($\tilde{C}_{J_{j,a},i}$) are solved independently, being the solutions of the three following mass conservation equations sampled at atmospheric station i:

$$\begin{cases} \frac{\partial}{\partial t}\left(\rho_{\mathbf{x},t}\tilde{C}_{E_{j,m},\mathbf{x},t}\right) + \nabla.\left(\rho_{\mathbf{x},t}\tilde{C}_{E_{j,m},\mathbf{x},t}\mathbf{v}\right) = \tilde{E}_{j,m}\,,\ \tilde{C}_{E_{j,m},\mathbf{x},t=0} = 0 \\ \frac{\partial}{\partial t}\left(\rho_{\mathbf{x},t}\tilde{C}_{OH_{j,m},\mathbf{x},t}\right) + \nabla.\left(\rho_{\mathbf{x},t}\tilde{C}_{OH_{j,m},\mathbf{x},t}\mathbf{v}\right) = -k_{j,m}[\tilde{OH}]_{j,m}\hat{C}_{j,m}\,,\ \tilde{C}_{OH_{j,m},\mathbf{x},t=0} = 0 \\ \frac{\partial}{\partial t}\left(\rho_{\mathbf{x},t}\tilde{C}_{J_{j,a},\mathbf{x},t}\right) + \nabla.\left(\rho_{\mathbf{x},t}\tilde{C}_{J_{j,a},\mathbf{x},t}\mathbf{v}\right) = -\tilde{J}_{j,a}\hat{C}_{j,a}\,,\ \tilde{C}_{J_{j,a},\mathbf{x},t=0} = 0 \end{cases} \quad (5)$$

with $\tilde{E}_{j,m}$ being a unit source or sink, $[\tilde{OH}]_{j,m}$ the a priori concentration field and $\tilde{J}_{j,a}$ the a priori photochemical rate. As the full mass conservation Eq. (3) has been linearised, $\tilde{E}_{j,m}$ is considered as a pulse source of a passive tracer (Eq. 5.1), whereas no source is applied while solving OH sink (Eq. 5.2) or stratospheric loss (Eq. 5.3). The overall modeled MCF concentration for station i at a time t, $C_{i,t}$ thus becomes a linear combination of the different response functions:

$$C_{i,t} = \alpha_0\tilde{C}_{0,t_0} + \sum_{j,m}\left(\alpha_{E_{j,m}}\tilde{C}_{E_{j,m},i} + \alpha_{OH_{j,m}}\tilde{C}_{OH_{j,m},i}\right) + \sum_{j,a}\alpha_{J_{j,a}}\tilde{C}_{J_{j,a},i}, \quad (6)$$

where $\tilde{C}_{0,t_0}$ is a global offset, j represents regions and m refers to all months between time t_0 and t. The unknowns are the scaling factors (α) of the response functions ($\tilde{C}$): $\alpha_{E_{j,m}}$ for monthly MCF surface sources and sinks, $\alpha_{\mathrm{OH}_{j,m}}$ for monthly OH concentrations, and $\alpha_{J_{j,a}}$ for annual stratospheric loss. The optimization relies on a classical Bayesian formulation where one minimizes a quadratic cost function $J(\alpha)$ between modeled and observed concentrations from one hand, and prior estimates and optimized estimates from the other hand, each term being weighted by variance/covariance matrices (see Appendix B). The new set of MCF sources and sinks inferred by the inversion for the 1979–2000 period is then used in a forward inter-annual simulation with LMDZ-INCA (with varying meteorology) to calculate an updated 3-D $\hat{C}_{\mathbf{x},t}$ field. This field allows the computation of new chemical response functions needed to perform the next inverse iteration. $\hat{C}_{n;\mathbf{x},t}$ converges to the inverse solution and gets closer to observed concentrations at each iteration.

In practice, this methodology is numerically costly because, for each iteration and 21 years of integration (1979–2000), it is necessary to calculate 252 chemical response functions per region inverted, which represents hundreds of hours of calculation on a supercomputer. Thus we reduced the time propagation of each OH pulse to 6 months (1 month of sink and transport + 5 months of dilution by transport only) and then extrapolated in time response functions toward their asymptotic value (Appendix C). We also have limited the number of iterations to 2, because the change of $\hat{C}_{n;\mathbf{x},t}$ between iteration 3 and 2 is rather small (<5%).

For source response functions, the calculation is performed only once as sources are linearly linked to concentrations once the problem is linearized (Eq. 5.1). However, in order to save computing time, we have limited the calculation of inter-annual source response functions to 1990–2000 period, and used the mean response functions of 1990–2000 for the 1980s. For time propagation, we proceed the same way as for chemical response functions (1 month of source and transport +5 months of dilution by transport only + extrapolation towards final value, see Appendix C).

Figure 4 shows chemical (Fig. 4a, b) and surface source response functions (Fig. 4c) at Barbados (RPB) for the period 1979–2000. Monthly pulses of chemical response functions are seasonal (Fig. 4a) and follow the trend of MCF in the atmosphere on longer timescales (Fig. 4b). There is also a significant variability from one year to the next due to transport of MCF emissions and concentrations. Source response functions (Fig. 4c) also show significant inter-annual variability linked to transport only (Fig. 4c).

To quantify inter-annual variability of source and chemical response functions, we calculated an index of inter-annual variability (IAV index). For each station and each month between 1979 and 2000 we first scale all chemical response functions to the asymptotic value of source response functions in order 1. to remove decadal changes of OH sink and 2. to compare both type of response functions. Then, for each response function, we compute the month of the maximum value and the corresponding maximum. The IAV index is then defined as the standard deviation of the maximum values across the 21 years of inversion (21 values) divided by the mean of the maximum values across the 21 years (same 21 values), expressed as a percentage. Thus, we get one value of IAV index for each station, each region (sources and sinks) and for each of the 12 months of the year. We report in Table 2 the region producing the maximum IAV index at each station, together with the month of the maximum of the response functions. Uncertainties attached to IAV index refer to standard deviation of monthly IAV index (12 values).

We find that IAV index of a given station is significant only when the maximum of the source/sink response function reaches the site during the first three months of propagation, and it is much larger when it occurs during the first month. After three months, the plume is mixed rather uniformly and the effects of transport variability vanish. Typical high indices larger than 50% occur when a source/sink region is located close to the station and reaches it during the first month of propagation, such as MHD with European emissions (Table 2). At MHD, winter pulses, associated with strong westerly transport, even show IAV indexes above 60%. Table 2 also shows that OH response functions have smaller IAV index than source response functions, except in the tropics, where they are of the same order of magnitude but less than 10%. The removal of MCF by OH is indeed a process occuring in the volume of the atmosphere, that maximizes in the mid-troposphere (using MOZART field) and

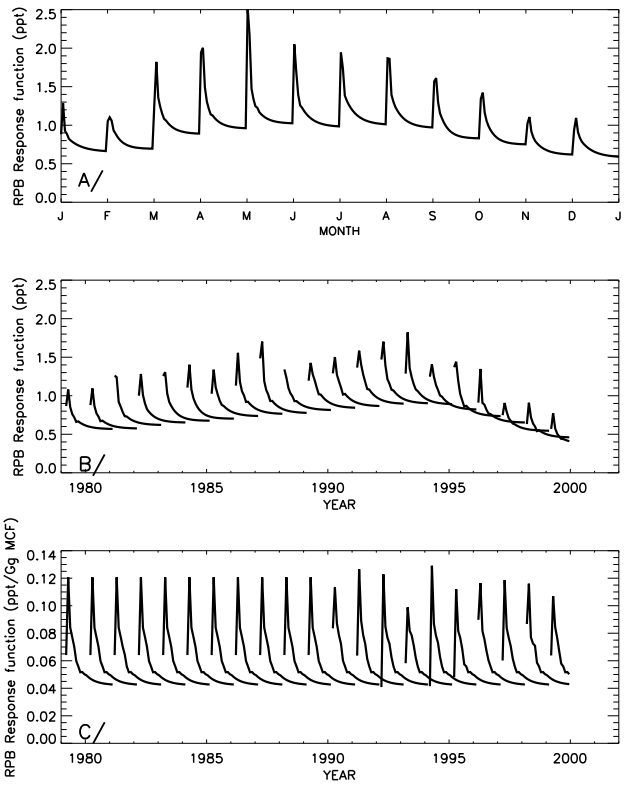

Fig. 4. Chemical and source response functions at Barbados station (RPB). Response functions represent the contribution to MCF concentration at one station from chemical sink or from a normalized 1-Gg source of MCF. Chemical response functions are positive because associated scaling factors are negative. **(a)** 12 monthly chemical response functions for year 1990 due to NH tropical OH (in ppt). **(b)** 21 chemical response functions for all march months between 1980 and 2000 due to NH tropical OH (in ppt). **(c)** Source response functions for all march months between 1980 and 2000 due to North America emissions (in ppt/Gg). IAV of transport has only been calculated for 1990-2000. For other years, mean response function over 1990–2000 is used.

therefore more remotely related to the surface stations than surface emissions. In the tropics, the IAV of the source response functions is small as most MCF sources are located north of 30° N. Using 4–10 stations remotely located from the main sources and sinks may thus underestimate the impact of inter-annual meteorology on the response functions and further smooth the inferred year-to-year variability of the MCF emissions. Optimization of another tracer with observation sites located close to emissions and/or within continental areas (e.g. SF_6 or CH_4), will probably lead to much larger IAV indexes. Finally, ocean pulses reach MCF stations mostly during the first or second month of emission, because of the marine or coastal position of stations. Thus, ocean pulses generate substantial IAV indices at stations such as ALT, SMO or PSA (Table 2). The impact of varying meteorology on the inversion results will be discussed in Sect. 3.

Table 2. Mean IAV index per station for main MCF source and sink (ocean) regions and OH sink region (in %). "MONTH" column indicates the month of the maximum of the response functions.

Station	Source Region	IAV Index	Month	OH Region	IAV Index	Month	Ocean Region	IAV Index	Month
ALT	Asia	6±3	2	NHN	3±1	3	NH_bor	22±3	0
NWR	North America	13±6	1	NHN	6±2	2	NH_bor	5±1	2
MHD	Europe	50±11	0	NHN	5±2	2	NH_bor	11±2	1
KUM	Asia	9±4	2	NHT	9±2	2	NH_bor, NH_temp	6±2	0
MLO	Asia	9±2	2	NHN	8±1	2	NH_temp, Trop	6±2	1
RPB	North America	9±3	2	NHN, NHT	8±2	1	NH_temp, Trop	7±2	0
SMO	SH	5±2	2	SHT, SHS	11±2	2	Trop	13±2	0
CGO	SH	23±4	1	SHS	4±1	2	SH_temp	10±3	0
PSA	SH	4±1	3	SHS	4±1	2	SH_aus	12±4	0
SPO	SH	5±1	2	SHS	3±1	2	SH_aus	6±2	1

2.5 Uncertainties

The choice of uncertainties on prior estimates (diagonal elements of **P)** is an important step of the inversion (see Appendix B). Uncertainties on OH concentration for the 4 latitude bands are set to ±100% each month in order to let OH be adjusted freely. Uncertainties on MCF sources are prescribed according to McCulloch and Midgley (2001) on an annual basis. Annual errors reported in percentage are in the range of 2–2.5% until the early 1990s but increase to 25% in 1999 as emissions decreased rapidly in the 1990s due to the application of Montreal protocol. Errors on monthly sources/sinks are supposed to be uncorrelated. Uncertainties on the ocean sink were set to ±100%.

The uncertainty on the observations (diagonal elements of **R)** comprises both the measurement error and the so-called representation error (Appendix B). Measurement errors were set according to the standard deviations given with ALE/GAGE/AGAGE monthly means. They range from 0.1 ppt to a few ppt. The representation error is caused by the inability of a model to properly reproduce the observations, due to various possible reasons including: too coarse horizontal resolution to capture local topography and aerology, unrealistic winds or vertical transport in the troposphere or in the planetery boundary layer, data selection, not allowing for MCF/OH feedbacks within a month, ... If one does not account for it, differences due to the representation error are inverted into inaccurate changes in sources and/or sinks. In particular for MCF, because emissions have rather small uncertainties, too much confidence in the ability of the model to reproduce the data will produce large year-to-year variations of the OH concentration. The representation error is difficult to evaluate although some attempts have already been made (Rodenbeck et al., 2003; Gerbig et al., 2003). As noticed in Prinn et al. (2001, 2005), part of the representation error is already included in the standard deviations provided with the observed monthly means. However, some issues, such as data selection to remove polluted events or varying meteorology in the 1980s are not included. Here, we used a simple approach to scale observational uncertainties, based on Tarantola (1987): starting from monthly errors attached to observations (varying in time), we reset all values smaller than 1 ppt to exactly 1 ppt, and then, we iteratively and globally scaled all monthly errors in **R** in order to fulfill the statistical chi-square requirement (Peylin et al., 2002):

$$\chi^2 = \frac{2J\left(\alpha_a\right)}{\nu} \leq\approx 1,$$

where α_a is the optimized state vector α at the minimum of J, and ν is the number of degrees of freedom, given by the dimension of the observation vector $\mathbf{y}_{obs}$ (Tarantola, 1987, p. 212). By doing so, we limit the information content of MCF observations to the extent our transport model is able to reproduce. In other words, we tend to limit the translation of representation errors into wrong OH fluctuations. We applied such an approach to an inverse set up with one global region for MCF sources, one global region for ocean sink, and one global region for OH sink with 4 stations from ALE/GAGE/AGAGE network, and then use the inferred uncertainties for all inversions. With this procedure, the initial errors increased by 20% with an overall minimum error of ±1.2 ppt for all months (see mean/min/max values for all stations in Fig. 1). For the test that includes NOAA/CMDL stations, monthly variances at these sites were calculated as the sum of an arbitrary ±5% error of MCF concentration at each site and of a ±3 ppt error to account for possible calibration issues between the two networks. Such choice leads to slightly larger uncertainties on average for stations from NOAA/CMDL network (Fig. 1).

2.6 Additional constraints

One additional constraint is added in the inverse procedure in order to prevent unrealistic monthly fluctuations in the inferred sources and sinks. Using Peylin et al. (1999) methodology, changes of the month-to-month differences in OH concentration are limited to 50% of the prior month-to-month

Table 3. Set up of the 16 inversions performed: number of observations sites used, Number of regions solved for, Error on observation, Error on prior estimates, Use of inter-annual chemical response functions, use of inter-annual source response functions.

INV I-XX	OBSERVATIONS	REGIONS	OBS ERROR	FLUX ERROR	Chemical IAV	Transp. IAV
01	10 REF + ALT, KUM, MLO, NWR, PSA,SPO,	13	REF	REF	YES	YES
02	4	6 1OH+4MCF+1OCE	REF	REF	YES	YES
03	4	13	No MMD	REF	YES	YES
04	4	13	No sums	REF	YES	YES
05	4	13	REF	* 0.5	YES	YES
06	4	13	REF	* 1.5	YES	YES
07	4	13	* 1.3	REF	YES	YES
08	4	13	* 0.7	REF	YES	YES
09 REF	4 CGO,MHD,RPB ,SMO	13 4OH+4MCF+5OCE	See sect. 2	2-25% MCF 100% OH	YES	YES
10	4	13	REF	REF	YES	1992
11	4 MHD polluted data	13	REF	REF	YES	YES
12	4	13	REF	Fixed MCF	YES	YES
13	4	13	REF	Fixed MCF 200% OH	YES	YES
14	4	3 1OH+1MCF+1OCE	REF	REF	YES	YES
15	6 REF + CMO + TRH	13	REF	REF	YES	YES
16	8 REF + ALT, KUM, MLO, NWR	13	REF	REF	YES	YES

differences. We did the same for MCF surface sources and sinks but set the limit only at 5% as these emissions do not present significant seasonal variations.

As we divided land sources into 4 regions, no explicit constrain is applied on the total sum of MCF surface sources. Thus, we added an additional constraint on this sum, given by flux and error estimates from McCulloch and Midgley (2001). Sensitivity test were performed to see the impact of these two additional constraints on the results.

3 Results

We present the results of an ensemble of 16 inversions (I-01 to I-16, Table 3). The reference inversion (I-09, Sect. 2 and Appendix A) contains 4 stations from ALE/GAGE/AGAGE network, and optimizes monthly MCF emissions over four regions (North America, Europe, Asia and SH), ocean sink over five zonal regions (see Sect. 2.2), and monthly OH concentrations over 4 latitudinal bands (NHN, NHT, SHT, SHS). As it is difficult to account quantitatively for all sources of uncertainty in a single inversion, we performed 15 additional sensitivity inversions, their set-up being summarized in Table 3. OH concentrations are analyzed in terms of mean concentration, year-to-year variations and long-term evolution that will be hereafter called "OH trend" as in previous studies[2].

[2]One has to notice that formally OH trend is actually OH growth rate, as defined in Appendix D. It is expressed in ppt/yr and reveals long-term evolution of OH concentrations.

3.1 Fit to observations

Figure 2 shows how the optimized model fits MCF observations at 6 stations (among 10, inversion I-01). Over all inversions, total χ^2 ranges between 0.2 and 1, which means that uncertainties are not too tight, because of loose prior errors put on monthly OH. "Prior" part of χ^2 (grouping prior estimates of OH sink, of stratospheric loss and of MCF surface sources and sinks) represents between 20 and 30% of the total χ^2, meaning that most of the optimisation relies on observations but that prior estimates still play a significant role, due to the small uncertainties on MCF sources. Although the fit to the observations is very good at most stations, the optimized model cannot reproduce properly the high MCF values in the early 1990s at NWR. NWR is an altitude site (>3000 m a.s.l.) and is thus hard to position properly in a CTM with a typical horizontal resolution of a few hundred kilometers in longitude and latitude, which tends to smooth surface topography. The contributions of the different stations to χ^2 ranges from less than 1% (ALT, KUM, PSA, SPO) up to more than 20% (MHD, NWR), whereas an evenly spread contribution would give 10% (Fig. 2). This means that a larger weight is put on MHD and NWR in the minimization of J.

Figure 5 plots observed minus optimized concentrations on a monthly basis (as in Krol and Lelieveld, 2003, Fig. 5) together with a 12-month running mean of the diffuerence

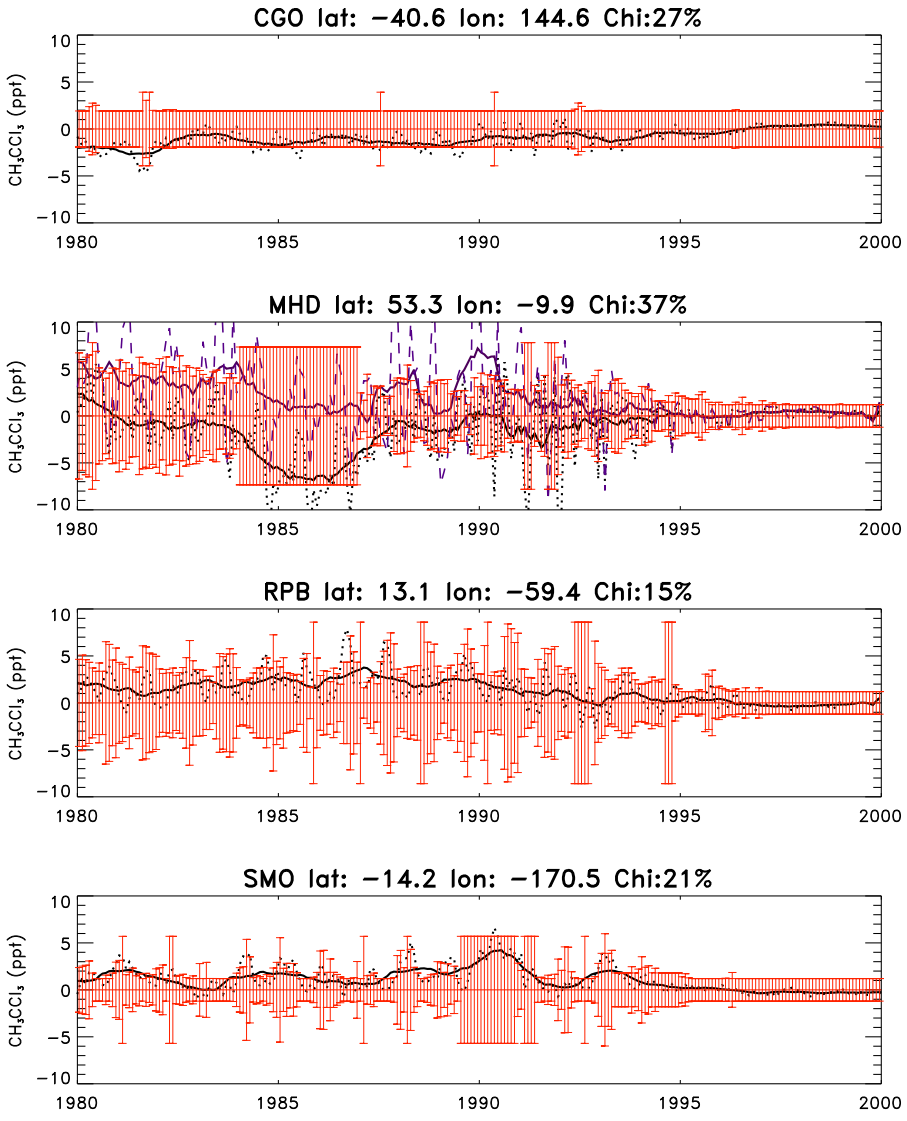

Fig. 5. MCF atmospheric residuals at 4 ALE/GAGE/AGAGE stations (in ppt): Differences between MCF observations and optimized MCF concentrations. 12-month running mean (solid lines) and monthly differences (dotted and dashed lines) are plotted. Observational uncertainties are in red. "Chi" stands for the contribution of the station to the Chi-squared statistics (in %). For Mace Head (MHD), purple lines represent the residuals that are obtained when polluted data are used (inversion I-11).

(as in Prinn et al., 2001, Fig. 4). For most stations, monthly residuals usually remain below 5 ppt, whereas smoothed residuals usually stay within ±3 ppt, except at MHD, with large mismatch observed in 1990–1992, when MCF concentrations are the largest. Also, no data were available at MHD during the 1984–1986 period. Thus, available measurements before and after this period were interpolated using Thoning et al. (1989) procedure. These concentrations were associated with much larger uncertainties, producing a poor fit of the optimized model. The same issue occurs at SMO in 1989–1991. Residuals at RPB and SMO show a positive long-term mean in the 1980s, balanced by negative mean residuals at CGO during the same period. This feature possibly indicates a too fast inter-hemispheric mixing that leads to an underestimation of the modelled concentrations in the northern hemisphere and to an overestimation of the modelled concentrations in the southern hemisphere. Such a bias in the residuals is also visible in Krol and Lelieveld (2003, Fig. 5) at RPB or CMO. It is reduced from the mid 1990s when the difference in MCF content between the northern hemisphere and the southern hemisphere becomes very small. Another hypothesis to explain this bias is the fact that we do not use inter-annual meteorology for transport in the 1980s, as mentioned in the text. The inversion does not completely correct for this because of substantial observational errors. Reducing observational errors,

Table 4. MCF global yearly emissions and uncertainties from mean inversion in Gg/yr. First uncertainty is returned by inverse procedure (internal uncertainty). Second uncertainty is the standard deviation of the results of the 16 inversions (external uncertainty). Third is global uncertainty. Prior estimates are from McCulloch and Midgley. Column 0H_15% shows MCF inverted emissions and uncertainties when OH monthly uncertainty decreased to ±15% instead of ±100% (see Sect. 4). Column OH FIXED shows inverted MCF emissions when OH is nudged to its prior monthly value.

Years	Mean Inversion	Prior	OH±15%	OH Fixed
1980	536±8.2/1.2/8.2	538±13	535.5±7.4	534.8±6.9
1981	542.4±8.2/1.4/8.3	549±13	532.2±7.4	526.4±6.9
1982	526.2±7.9/1.7/8.1	523±12.5	520.9±7.3	516.3±6.8
1983	536.7±8/2/8.2	536±12.6	535.9±7.4	535±6.8
1984	576.1±9.1/3.1/9.6	585±14.7	574.9±8.7	573.1±8
1985	586.9±8.8/2.8/9.3	593±14.1	580.6±8.4	575.5±7.8
1986	592.5±8.8/2.3/9.1	602±14.1	578.5±8.1	573.8±7.4
1987	611.3±9/2.9/9.5	623±14.7	604.5±8.3	607.7±7.5
1988	653.3±9.8/2.3/10.1	666±16.3	647.1±8.7	648.6±7.8
1989	679.3±9.9/2/10.1	691±16.5	655.5±8.5	644.4±7.6
1990	704.9±10.3/2.5/10.6	718±17.1	692.9±9.2	682.8±8.2
1991	635±10.3/1.9/10.5	635±17.2	629.9±9.2	632±8.4
1992	572.5±9.2/2.1/9.4	593±14.7	573.5±8.3	581±7.6
1993	372.3±13.5/3.7/13.9	380±27.3	368.4±10.9	377.5±9.4
1994	270.5±11.4/3.4/11.9	283±21.1	268.4±9.4	273.7±8.1
1995	212.5±10.7/2.4/11	234±20	203.5±8.4	201.3±7.1
1996	102.7±8.3/2/8.6	93.5±15	103.2±6.9	101.6±5.9
1997	45±3.4/0.9/3.5	39.5±5	46.6±3.3	47.4±3.1
1998	27.3±3.4/0.8/3.5	24.2±5	28.3±3.3	29.1±3.1
1999	22.9±3.4/0.5/3.4	21.4±5	24.1±3.2	25.4±3.1

would reduce this bias but at the prize of a correcting a possible transport problem by additional OH variations.

As mentioned before, no selection criterion is applied to model outputs, mostly because we did not use inter-annual meteorological forcings before 1990. In 3-D inversions, this could be critical point. It is still widely discussed between modellers and experimentalists. In order to test the influence of this limitation on OH variability, we did a sensitivity test at MHD by using data with polluted events included. We chose MHD because this is the station where polluted data and non-polluted data are the most different (Prinn et al., 2000). The change in the fit is significant (Fig. 5): the optimized model is overestimating the variability when using MHD non-polluted data (especially in 1990–1992) and is largely underestimating it when using polluted MHD data (especially in the 1980s, when no inter-annual meteorology is used). When inter-annual meteorology is used, LMDZ catches well the phase of MCF signals but underestimates their amplitudes due to a too fast mixing of the low troposphere. However, as can be seen in Sect. 3.3 of the paper, the impact on OH variability is rather small which means that the issue of data selection is not critical in this work. The residuals that are obtained in this study could be reduced by using inter-annual meteorology for the whole period and by applying a consistent selection of model outputs.

3.2 MCF emissions

Table 4 gives the global optimized MCF emissions for the mean of the 16 inversions, and the associated the internal error (mean error returned by the 16 inversions) and external error (standard deviation of the emissions given by the 16 inversions). The global uncertainty is computed assuming that internal and external uncertainties are independent. Mean emissions remain within $\pm 1\sigma$ of McCulloch and Midgley (2001) inventory. Integrated emissions over 1979–2000 are reduced by 1.1% (about 108 Gg) compared to inventory, mainly between 1985–1995. Global error reduction is 35%±5%, indicating that MCF observations contribute efficiently to improving emission estimates. However, the error reduction is limited by the rather tight prior errors of MCF emissions (2–25%). After 1996, both prior and posterior emissions become smaller than 20 Gg/yr, but the prior uncertainties on emissions also get small in parallel (±5 Gg/yr). We did a special inversion in which we extend the period of inversion of I-01 (10 stations) to the end of 2002 using only NOAA/CMDL stations after 1999. In this case, when increasing the prior uncertainties up to ±15 Gg/yr (about ±100% of the global prior emission) for the period 1997–2002, we discovered that global MCF emissions increase by 13 Gg/yr (+3 over Europe, +4 over Asia and +6 over North America). For the 2000–2002 period, optimized MCF emissions are found to be 7.1±2.6 Gg/yr over Europe, 7.8±2.8 Gg/yr over Asia and 11.8±3.8 Gg/yr for all North and Central America. For Europe, these emissions stand between the large emissions inferred by Krol et al. (2003) (20 Gg/yr) and the small emissions inferred by Reimann et al. (2005) (0.3–3.4 Gg/yr). There is no agreement so far on European residual MCF emissions inferred from atmospheric observations. For North America, Millet et al. (2004) find US emissions of 5.1 Gg in 2001 and 3.7 Gg in 2002 based on MCF data analysis, which is about twice the Li et al. (2005) estimates (2.2 Gg/yr for the 2001–2002 period) based on TRH measurements. Our estimate for North and Central America MCF emissions (11.8±3.8 Gg), even if covering a larger area than US territory only, appears to be much larger. One possible reason could be an underestimation of other emissions (North Asia and Southern Hemisphere) as the global MCF emissions of 20±5.5 Gg+/yr is more constrained by the inversion than the regional estimates, due to the small number of MCF stations. It would be interesting to include recent AGAGE data in our inversion (when available) to see their impact on European and North American residual MCF emissions after 2000.

Finally, the external error is usually much smaller than internal error (up to a factor of 10), meaning that the sensitivity test performed do not dramatically change the MCF emissions. In 1993–1994, both internal and external errors

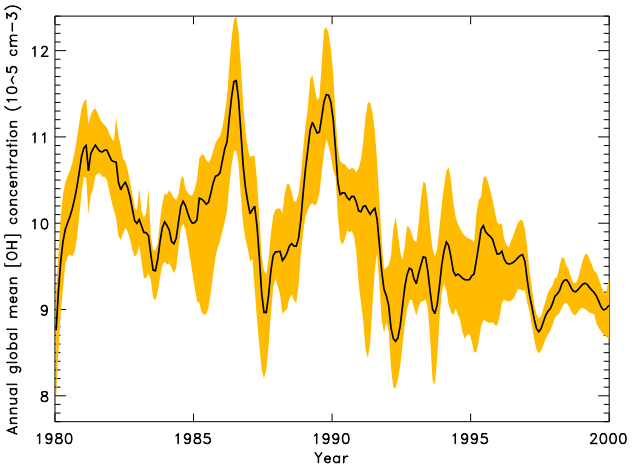

Fig. 6. Global deseasonalized OH variations from 1980 to 2000 in [$\times 10^5$ cm^{-3}]. Solid line is the mean of all inversions performed ("mean inversion"). Grey zone represent the envelope of all 16 inversions.

increase due to larger prior error on emissions estimates ($\pm$27 Gg in 1993): emissions being less constrained, posterior uncertainty is larger and the spread between the 16 inversions increases.

3.3 Global OH variations

Figure 6 presents the inverted, deseasonalized variations of global OH concentrations. They range from 8.0 to 11.8$\times 10^5$ cm^{-3} with an average of 9.8$\pm$0.9$\times 10^5$ cm^{-3} during 1980–2000 period, that compares well with prior studies (Table 1). The grey area in Fig. 6 represents the envelope of all 16 inversions. Our mean OH concentration is close to Prinn et al. (2001) estimate (i.e., 9.4$\pm$1.3$\times 10^5$ cm^{-3}), being only 5% larger. Yearly optimized [OH] are reported in Table 5. First, we infer large fluctuations of [OH] of 8.5$\pm$1.0% on average from one year to the next, and up to 20% in 1985–1987. All 16 inversions give large year-to-year OH variations. Second, we infer a negative long-term trend in [OH] of $-0.7\pm0.2\%$ yr^{-1} after 1980 (calculated from annual averages). These calculations were performed from the annual means. The shape of OH variations shows a change in the trend in the late 1980s. A small positive trend is found for the 1980s ($+0.1\pm0.4\%$ yr^{-1}) and then a negative trend is found for all posterior periods ($-1.0\pm0.4\%$ yr^{-1}). This negative trend is decreased (in absolute value) to $-0.5\pm0.4\%$ yr^{-1} in the late 1990s.

3.4 Global ocean sink

The IAV of MCF ocean sink is only slightly modified compared to the estimate of Wennberg et al. (2004), with about 1% increase of the sink in the 1980s and 1–2% decrease after the late 1990s. However, the error reduction is important (60%) for the ocean sink, meaning that MCF observations do bring information on this process. Not accounting for ocean sink does not change IAV of OH concentrations but leads to an increase of the mean inferred OH concentration by $+0.5\pm0.2\times 10^5$ cm^{-3} from 9.8 to 10.3$\times 10^5$ cm^{-3}, and to an increase of OH trend of 30% (in absolute value) from -0.7 yr^{-1} to -1.0 yr^{-1} for the 1980–2000 period. The fit to MCF observations is obviously improved by accounting for the ocean sink because degrees of freedom are increased in the inversion. This simple sensitivity test could be refined by testing another ocean sink representation such as Yvon-Lewis and Butler, 2002) as in Prinn et al. (2005).

Table 5. OH annual and global mean concentrations and uncertainties from mean inversion in [$\times 10^5$ cm^{-3}]. First uncertainty is internal uncertainty. Second is external uncertainty. Third is global uncertainty. Column 0H_15% shows MCF inverted emissions and uncertainties when OH monthly uncertainty decreased to $\pm$15% instead of $\pm$100% (see Sect. 4).

Years	Mean inversion	OH$\pm$15%
1980	10.1$\pm$0.9/0.3/0.9	9.6$\pm$0.4
1981	10.9$\pm$0.8/0.2/0.8	10.1$\pm$0.3
1982	10.5$\pm$0.8/0.2/0.8	10.1$\pm$0.3
1983	9.5$\pm$0.7/0.2/0.7	9.7$\pm$0.3
1984	10.2$\pm$0.8/0.2/0.8	9.8$\pm$0.3
1985	10.2$\pm$0.8/0.4/0.9	9.9$\pm$0.4
1986	11.7$\pm$0.9/0.4/1	10.2$\pm$0.5
1987	9$\pm$0.7/0.3/0.7	9.4$\pm$0.3
1988	9.8$\pm$0.7/0.30.8	9.5$\pm$0.4
1989	11.1$\pm$0.8/0.3/0.9	10.3$\pm$0.4
1990	10.3$\pm$0.8/0.2/0.8	10$\pm$0.3
1991	10.2$\pm$0.8/0.4/0.9	9.6$\pm$0.4
1992	9$\pm$0.7/0.3/0.7	9.2$\pm$0.3
1993	9.2$\pm$0.7/0.3/0.8	9.4$\pm$0.4
1994	9.4$\pm$0.7/0.3/0.8	9.5$\pm$0.4
1995	9.9$\pm$0.7/0.3/0.8	9.7$\pm$0.4
1996	9.5$\pm$0.7/0.2/0.7	9.7$\pm$0.3
1997	8.8$\pm$0.7/0.1/0.7	9.4$\pm$0.2
1998	9.3$\pm$0.7/0.1/0.7	9.5$\pm$0.2
1999	9.2$\pm$0.7/0.2/0.7	9.4$\pm$0.3

3.5 Global stratospheric loss

The stratospheric loss of MCF by photolysis is optimized yearly in our inversion, and only gets slightly modified compared to prior estimate (5–10% change). Inferred variations (not shown) do not present inter-annual variability but a slow decadal change. As suggested in Krol et al. (2003) and in Prinn et al. (2005), we find that stratospheric loss slowly increases from 1979 to mid 1993 and then decreases, following MCF concentration increase/decrease with a time lag of around 1–2 years, due to transport from the troposphere to the lower stratosphere.

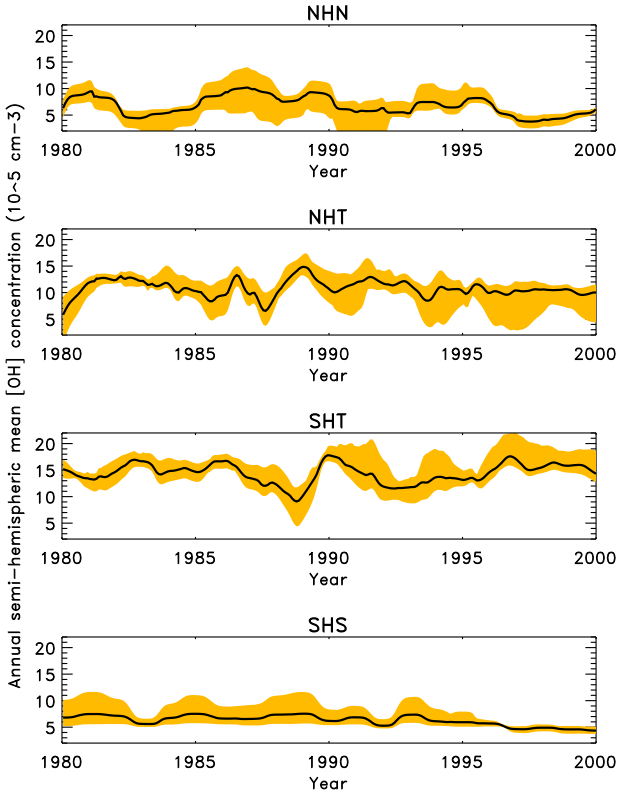

Fig. 7. Semi-Hemispheric deseasonalized OH variations from 1980 to 2000 in [$\times 10^5$ cm^{-3}]. Solid line is the mean of all inversions performed ("mean inversion"). Grey zone represent the envelope of all 16 inversions.

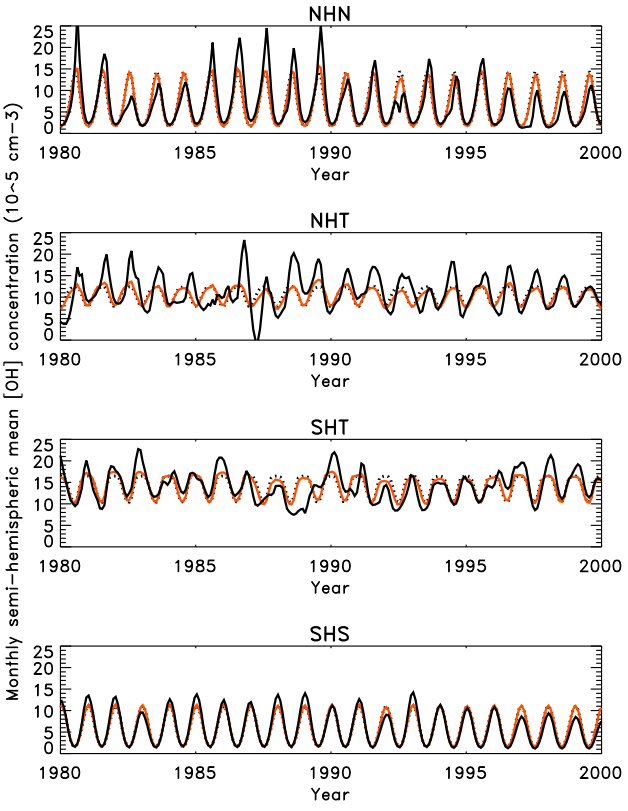

Fig. 8. Semi-Hemispheric monthly OH concentrations for the four regions of the standard inversion I-09 (in [$\times 10^5$ cm^{-3}]). Prior estimate from MOZART model (dark dotted line) is plotted with optimized model for the standard case I-09 (dark solid line) and for the $\pm$15% (see section 4, red solid line).

3.6 Latitudinal OH variations

OH variations are solved monthly for four latitudinal bands: 90° N–30° N (NHN), 30° N–0° (NHT), 0°–30° S (SHT), 30° S–90° S (SHS). Deseasonalised optimized OH variations (Fig. 7) shows that the largest OH changes occur in the tropical bands ($\pm$15% on average and up to 50%). Smaller variations are detected in NHN ($\pm$8% on average, up to 16%) and SHS ($\pm$4% on average, up to 8%). This is consistent with atmospheric chemistry being more active in the tropics than at high latitudes. A large spike of [OH] in 1985–1987 is evenly found in the two tropical bands, whereas the 1989–1991 spike is mostly attributed to southern tropics (SHT). We checked that the different bands are not systematically positively or negatively correlated. For instance, NHT is positively correlated to SHT in 1985–1987 but negatively correlated in 1988–1990. Compared to the prior MOZART OH field, MCF optimization largely reduces mean [OH] in NHN ($-$21%) and in NHT ($-$32%). In the southern hemisphere, mean [OH] is slightly reduced in SHT ($-$3%) and increased in SHS (+36%). This leads to higher mean [OH] in the SH compare to the NH (N/S ration of 0.87). On a monthly basis (Fig. 8), the MCF optimization increases the amplitude of the OH seasonal cycle by 20%, yet with a decrease of 25% for the NHN and increases in other latitudinal bands (+7% for NHT, +27% for SHT and +21% for SHS). Changes occur in all seasons in the tropical bands but decrease in NHN and increase in SHS occurs mainly during summer months (Fig. 8). Also visible on Fig. 8 is the 1985–1987 anomaly, mostly due to NHT, and the 1989–1991 anomaly, mostly due to SHT. On a decadal basis, we find that the OH trend is different within the four latitudinal bands. The small increase in OH found during the 1980s (+0.1$\pm$0.4% yr^{-1}) is mostly due to northern hemisphere (NHN and NHT), which confirms a result found by Prinn et al. (2001), whereas southern hemisphere shows zero to small negative OH trend. The decrease in OH of the 1990s is present at all latitudes but is more sensible in the southern hemisphere (SHT and in SHS), with an acceleration in SHS after 1993 and in SHT after 1998, partly compensated by a positive trend in NHT after 1993 and in NHN after 1998 (Fig. 7).

We analyzed the correlation of errors between monthly sources or sinks, as returned by the inverse procedure. We report in Table 6 the average correlation matrix (over the 21

Table 6. Error correlations between sources and sinks of MCF: 4 source regions (MCF-NA for North America, MCF-EUR for Eurasia, MCF-SH for southern hemisphere), 4 OH sink latitudinal bands (NHN, NHT, SHT, SHS, see text), 5 ocean zonal bands (NH_bor, NH_temp, Trop, SH_temp, SH_aus, see text) and one global stratospheric region (STRATO). Correlations below 0.2 in absolute value are not shown.

	MCF-NA	MCF-EUR	MCF-ASI	MCF-SH	OH-NHN	OH-NHT	OH-SHT	OH-SHS	OCE	STRATO
MCF-NA	1.00									
MCF-EUR	-0.22	1.00								
MCF-ASI	-0.23	-	1.00							
MCF-SH	-	-	-	1.00						
OH-NHN	-	-	-	-	1.00					
OH-NHT	-	-	-	-	-0.48	1.00				
OH-SHT	-	-	-	-	-	-0.60	1.00			
OH-SHS	-	-	-	-	-	-	-0.39	1.00		
OCE	-	-	-	-	-	-	-	-	1.00	
STRATO	-	-	-	-	-	-	-	-	-	1.00

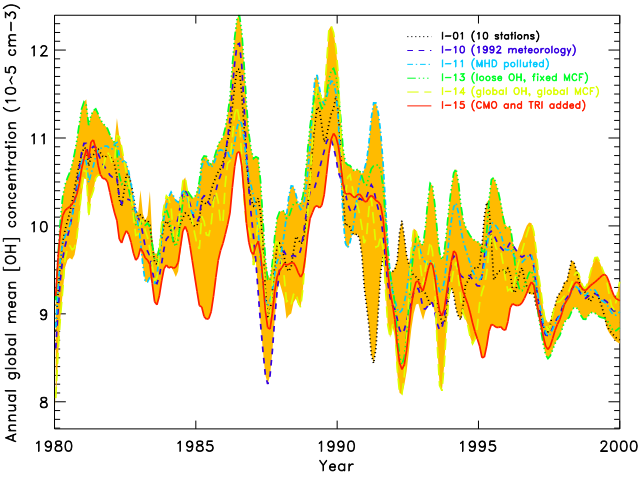

Fig. 9. Global deseasonalized OH variations from 1980 to 2000 for the sensitivity tests producing the largest changes compared to the mean inversion: using 10 stations (I-01, dotted line), using a recycled year (1992) for meteorology (I-10, short-dashed line), using loose OH priors and fixed MCF emissions (I-13), increasing uncertainties on OH concentrations and fixing MCF to priori values (I-11, long-dashed line), and solving only for 1 global source region and one global OH concentration each month (I-14 solid line). Grey zone is the envelope of all 16 inversions.

years of inversion) between all sources and sinks: 4 source regions, 4 OH sink regions, 1 global ocean region and 1 global stratospheric sink. Significant error correlations mean that regions can hardly be separated by inversion and that only a linear combination can be safely interpreted. For MCF emissions, we do not find significant correlations of errors, the largest negative correlation being −0.23. Significant negative error correlations occur between OH regions NHT and SHT (−0.60±0.07, p=0.01). For NHT and NHN we found a negative error correlation (−0.48±0.11) but at the limit of significance (p=0.08). An important result here is that no significant error correlations were found between sources of MCF and sinks of MCF, indicating that these quantities can be optimized separately. MCF emissions are surface fluxes whereas OH sink is maximum in the mid-troposphere, which induces a time lag of at least a few weeks between them and limits possible error correlations.

We investigated further this issue by calculating the full variance/covariance matrix, on a monthly basis (Pa matrix in Appendix B). We do find small error correlations above 0.2 (in absolute values) between sources and sinks on a monthly basis (e.g. European source correlated with Northern Hemisphere North OH sink), but only for some summer months of some years. When calculating error correlations on a yearly basis, the overall correlation is at largely reduced (maximum correlations of −0.1 to −0.15) because most of the months give small error correlations. Moreover, the highest monthly error correlations between sources and sinks (around −0.25) stands between MCF regions (mostly Europe) for some summer months and OH sink for the current and the previous months (0 to 3 months before). Such a time lag can also be observed in Table 2, in which the MONTH column gives the month of the maximum of the response function at one station. One can observe, for instance, that for MHD, the impact of the MCF emissions is maximum during the month of emission, whereas the impact of NHN OH sink is maximum 2 months after the OH pulse. The situation is more equilibrated in the tropics where MCF emissions and OH sink have a maximum impact at about the same number of months after the pulse occur. This can be explained by two opposed factors : the faster vertical transport in the tropics and the larger distance of surface stations to MCF sources in the tropics compared to northern mid-latitude stations. In other words, errors on MCF sources and sinks are more correlated in the tropics and/or for summer months, consistently with what can be expected from transport features. But the overall, yearly error correlations between sources and sinks

remain smaller than 0.2 in absolute value (−0.2 in reality), because response functions are significantly shifted in time and in shape.

3.7 Sensitivity tests

All the 16 inversions performed (Table 3) consistently return similar OH variability over the whole period 1980–2000 (Fig. 9). In few cases, some inversions produce distinct changes in amplitude and/or phase of global OH but only for short periods of 1–3 years.

Adding 6 NOAA/CMDL stations produces some phase differences (Fig. 9). The large drop in OH in 1990–1992 is opposite in phase with the mean inversion when the mountain site of NWR is used. Observations at NWR being high in MCF in the early 1990's compared to the prior model (not shown), an increase in OH is inferred in NHT, compensated by a decrease in OH in SHT (Fig. 7). Using CMO and TRH stations (I-15) produces a reduction of 15% of OH variability, together with a reduction of $0.3\times10^{-5}\,cm^{-3}$ of mean OH concentrations over 1980–2000 and a small reduction of long-term trend ($-0.6\%.yr^{-1}$ instead of $-0.7\%.yr^{-1}$) compared to mean inversion. This reduction is due to the fact that CMO is slightly higher in MCF than MHD in the model world, producing a decrease in the required mean OH. Using MHD data with pollution events included (I-11) does not significantly change OH variability, although it produces a spike of OH in 1991–1992, when MCF concentrations and variability reaches a maximum at MHD station.

Varying meteorology can also produce significant changes in inferred OH variations (I-10). When reusing the meteorology of a given year to calculate source response functions instead of actual meteorology, we found that repeated use of the 1992 meteorology was producing the largest changes in OH compared to the mean inversion. Year 1992 is a post-Pinatubo year during which reduced incoming radiation and temperature (Hansen et al., 1996) may have perturbed atmospheric transport. Using 1992 meteorology repeatedly increases the OH drop in 1987 by 50% and decreases the 1990–1992 spike by a factor of 2. However, our methodology, with linearized chemistry, may underestimate the impact of meteorology because we can only evaluate the impact of inter-annual transport on OH variations and not the impact of meteorology and radiation on OH production (Warwick et al., 2001). Inverting for a tracer with more coastal stations, as MHD, or continental sites may increase the influence of meteorology, as noticed for IAV index. Finally, note that the optimized Chi-Squared is smaller when using inter-annual meteorology compared to recycled one.

When the prior error on OH is multiplied by a factor of 2 while MCF emissions are tightly nudged around their prior value (I-13), the inverted OH variability increases by 22% on average, with no significant phase differences. Lower OH concentrations in the late 1990s and higher concentrations in the 1980s are then found compared to the mean inversion (Fig. 9). When solving only for 1 global OH region, 1 global MCF source region and 1 global ocean region (I-14), OH variability is increased by 11%, indicating that the impact of aggregation error is significant and tends to emphasize OH variations. Aggregation error occurs when an inverse procedure only solves for one scalar factor for an ensemble of model cells in space (making a region) and/or in time (Kaminski et al., 2001). Then if the space and/or time pattern is wrong, the inversion may scale the region source/sink for wrong reasons because of this hard constrained put on aggregated model cells. A solution to limit the aggregation error is to largely increase the number of regions solved for, and to provide soft constrains in order to regularize the inverse problem (Enguelen et al., 2002). Such soft constrains can be error correlations in the flux space (off diagonal elements of P matrix, see appendix C). Setting error correlations that are physically based is not an easy task, and several groups are currently working to produce consistent variance/covariance matrices of error based on biogeochemical models (Peylin et al., 2005; Rodenbeck et al., 2003). Anyhow, the problem is always to find a compromise between the quantity of available information in the observations and the number of degrees of freedom in the flux space. If one has only a small number of observations, it may appear that soft constrains will almost turn into hard constrains (error correlations very close to 1). In this case, it makes sense to directly use hard constrains, that is to solve for large regions. Considering 1/ the small number of available MCF stations over the 20 years, 2/ the fact that OH sink is 3-dimensional and 3/ the very large computing time that were necessary to address inter-annual variability, we chose to solve only for 4 OH regions and 4 MCF regions, knowing that we do not fully address the issue of aggregation error.

Decreasing prior error on MCF emissions by a factor of 2 reduces OH variability by 15% (I-05). Removing additional constraint on the sum of MCF emissions (I-04) leads to a decrease of 7% of OH variability associated with a reduction of 2.4% (−226 Gg) of the integrated source over 1980–2000, twice as much as in the standard case. Finally, suppressing constraints on month-to-month variations (I-03) or modifying observation errors (I-07, I-08) only changed OH variability by less than 5%. In particular, not applying the scaling of observational uncertainties (I-08) only slightly modifies OH inferred variations.

Overall, the 16 inversions show substantial OH variability in the atmosphere, with ±20% changes at maximum around the mean inversion, choice of MCF stations and meteorology being the more sensitive parameters of the inverse set-up. One noticeable point is that the phase of OH variations is a rather robust result among the different tests except for short time periods of 1–2 years. Finally, in any case, the variability induced by the 15 sensitivity tests (external error) stays much smaller than the error returned by the inverse procedure (internal error).

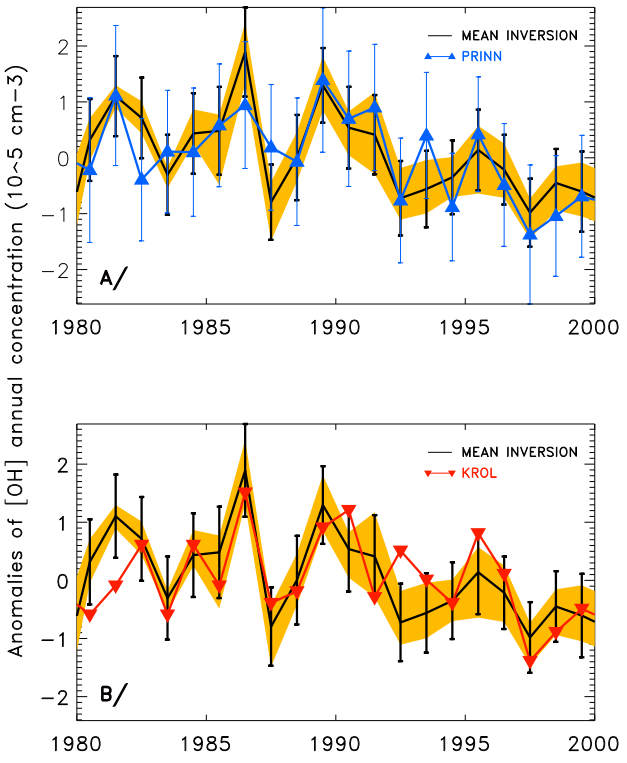

Fig. 10. Annual global OH anomalies from mean inversion (solid line) compared with estimates from Prinn et al. (2001) **(a)** and from Krol et al. (2003) **(b)**. Grey zone is the envelope of all 16 inversions.

3.8 Comparison with other studies

The results of the mean inversion are compared with Prinn et al. (2001), Krol et al. (2003), Dentener et al. (2002) and Montzka et al. (2000) hereafter referred as PR, KR, DE, and MO. At the global scale, Fig. 10 compares the yearly average optimized OH anomalies together with PR (Fig. 10a) and KR (Fig. 10b) results. PR, KR and our results show significant similarities in phase (R=0.70±0.07, p=0.001 with PR, and R=0.64±0.04, p=0.005 with KR) and in amplitude. Yet, we infer slightly higher OH mean abundance than PR and KR but similar magnitude and phase variations. Interestingly, inversion I-05 with uncertainties on MCF emissions divided by a factor of 2 presents larger correlations with PR and KR (R=0.85 and R=0.73, respectively). This is consistent with the fact that PR and KR do not optimize MCF emissions, which corresponds more to a set-up in the inversion with tighter MCF emissions (I-05). Overall, Wwe found a positive OH trend in the 1980s and a negative trend in the 1990s as in PR and KR. A mean value of -0.7% yr^{-1} (this work) is close to the trend reported by PR (-0.64% yr^{-1}) for the same period 1980–2000. For the 1980s, we found a positive trend in [OH] ($+0.1\%$ yr^{-1}) that is much smaller than PR and KR, but closer to DE ($+0.28\%$ yr^{-1} for 1979–1993). For DE, this small positive trend is due to stratospheric ozone and meteorological variability. For the 1990s, the decrease in [OH] inferred by inversions is smaller than those of both studies (by at least 30%). Yet, the trends in OH inferred by all three studies are consistent with each other considering their respective errors bars.

We calculated a N/S hemispheric OH ratio of 0.85 after optimization (Table 1), which is close to MO and PR estimate (0.88 and 0.87, respectively) and smaller than KR one (0.98). A larger depletion in Ozone in the SH compared to the NH due to Antarctic ozone hole could enhance UV light in the high troposphere and therefore enhance OH production in southern Tropics (Brenninkmeijer et al., 1992). We do find enhanced summer OH concentration in SHS as noticed previously. This result agrees with conclusions inferred from ^{14}CO measurements (Brenninkmeijer et al., 1992) but disagrees with recent modeling studies inferring more OH in the NH due to higher NO_x levels (Lawrence et al., 2001; Hauglustaine et al., 2004). Note however that we have considered geographical equator as in KR and in PR but not as in MO who have separated NH from SH at the level of ITCZ. This tends to increase SH OH average concentration as ITCZ average position is around 6° North (Holton, 1979). In Table 1, one can also observe the rather good agreement in NH and SH mean MCF content between PR, KR and this study.

4 Analysis and discussion

We address here the fundamental question of whether it is possible or not to use MCF to infer useful information on OH variations. Like for earlier studies, but using here a 3-D model and optimizing both OH and MCF sources with varying meteorology, we inferred substantial year-to-year variations of OH. It has been suggested by KR that such large variations may arise from model shortcomings, and they hypothesized that varying meteorology, varying emissions, or using a CTM with a higher resolution may reduce OH variations. We tested those three hypotheses. First, we found that varying meteorology as opposed to recycling transport fields, does not reduce the average amplitude of OH fluctuations beyond short time scales (<3 years). Second, we tested that letting emissions be inverted as well as OH does not alter the inference of large fluctuations, when prior errors on OH are kept loose. This result is insensitive to the prior error assigned within realistic bounds to the MCF emissions. Third, we tested that using a higher resolution model than in former studies did not change qualitatively the inferred OH variability. Finally, adjusting a stratospheric loss term only impacts OH changes on a decadal basis, but not from one year to the next.

What drives the large inverted OH inter-annual variations inferred by inversion? It is important to remark that the atmospheric observations originally contain a significant inter-annual variability. This is illustrated in Fig. 11 by the average MCF growth rate at four ALE/GAGE/AGAGE stations.

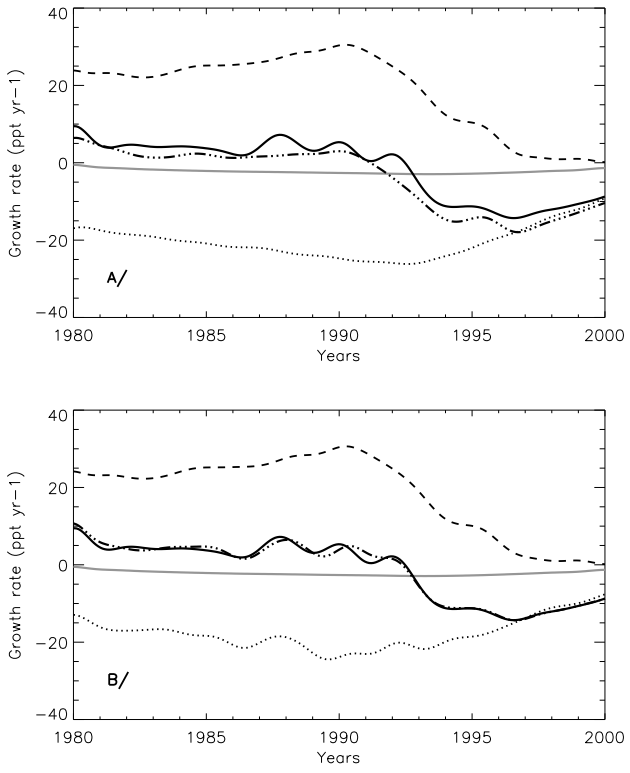

Fig. 11. Average Growth rate of MCF concentrations calculated from stations of ALE/GAGE/AGAGE network (CGO, MHD, RPB, SMO). Observed growth rate (solid line) is plotted together with total modeled growth rate (dotted-dashed line), which is the sum of growth rate due to MCF emissions (dashed line), OH sink (dotted line) and stratospheric loss (solid grey line). **(a)** Prior model. **(b)** Inversion I-09.

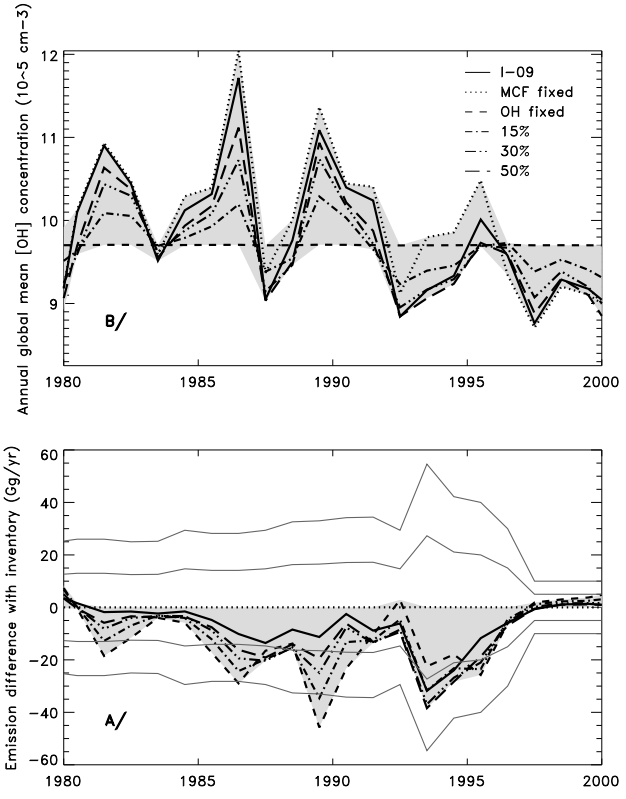

Fig. 12. MCF emission differences with inventory **(a)** and OH variations **(b)** for inversions with smaller prior OH uncertainties compared to I-09 (solid line): ±50% (long dashed line) ±30% (dashed 3-dotted line), ±15% (dashed 1-dotted line), and OH fixed (short-dashed line). A case with fixed MCF emissions and ±100% error on OH field is also plotted (dotted line). See text for further details.

It can be seen that the prior modeled growth rate matches the observed one for decadal changes. This is because the long-term sink is mostly determined (with a lag) by MCF emissions trends, OH trend being small compared to changes in MCF concentrations on the long-term (Appendix E). However, an overestimated mean prior OH sink causes a negative bias in the mean prior MCF growth rate (Fig. 11a). The optimization corrects for that mean bias, and greatly improves the fit to the inter-annual changes (Fig. 11b). The fit to the inter-annual data incurs to the OH term, because prior OH uncertainties are much larger than prior MCF emission uncertainties. For instance, the largest anomalous OH variations occur in 1985–1987 and 1989–1991 in order to match positive anomalies in MCF growth rate, which have no counterpart in the emission inventories.

To what extent uncertainties in annual emission inventories make the inferred OH changes robust? In order to answer this question, we tightened the a priori OH uncertainties from ±100% down to ±1%. Smaller prior errors on OH imply larger inter-annual variations in MCF emissions to match the observations (Fig. 12a). The inter-annual MCF emissions remain within 1-σ errors of the inventory estimates as long as the prior OH error is no tighter than ±50% (except in 1987 and 1989). A 2-σ error criteria is met for the MCF emissions as long as prior OH errors remains above ±15%. In other words, allowing for solutions where MCF emissions can deviate within 2-σ from inventories from one year to the next translates into smoother OH anomalies. A 2-σ criterion is statistically very unlikely to happen but one can notice that the 2-σ bound is only reached once over the 22-year period in 1989 for the 15% case. In that last case, up to 65% of the OH year-to-year variations can disappear (Fig. 12a). Also, seasonal OH variations are largely reduced compared to the reference inversion of Sect. 3 and stay much closer to prior values (Fig. 8). We believe however that the MCF sources being intimately linked to the global high-technology industrial activities likely varied smoothly, although pseudo-annual cycles due to endogen causes are observed in some innovative industries such as semiconductors production, and may have modulated MCF emissions in the past (NCI, 2003). Reducing OH year-to-year variations improves the consistency of OH fields as inferred by MCF with methane cycle (Dentener et al., 2002).

To what extent do uncertainties in long-term emission inventories make the inferred OH trends robust? This question was partly addressed by Krol et al. (2003) and Wang et al. (2004). As shown above for inter-annual time-scales, there is also a correlation between inverted OH and MCF emissions decadal trends. Setting tighter uncertainties on OH leads to an increase of MCF emissions after 1996 and before 1982 of 23 Gg, and to a decrease of 230 Gg between 1982 and 1996 (for the ±15% case). Overall the unbalance between the 1980s and the 1990s is about 207 Gg (±15% case), corresponding to a global reduction of integrated MCF emissions over 1979–2000. Conversely, allowing for MCF emissions to evolve on a decadal basis within 2-σ of inventories (±15% case) reduces the absolute magnitude of the OH trends by about 60% over the 1979–2000 period (-0.3% yr^{-1} v.s. -0.7% yr^{-1}). However, in all inversions performed here, we found that OH trend is neutral to positive in the 1980s and negative since the early 1990s.

Finally, as the source of MCF becomes small after 1997, the atmospheric gradients also become tiny and increasingly difficult to interpret. If the errors on emissions are kept proportional to the emissions themselves, then the atmospheric growth rate must be explained by OH changes, and we must infer a reduction of OH after 1995. Conversely, larger errors on the inventoried emissions than those in Fig. 12a, would translate into a smaller inferred OH drop post 1995. This sensitivity study shows that the quality of the inventory data, both in terms of accuracy and precision, is critical to infer OH changes from MCF observations.

5 Conclusions

Overall, the results of MCF inversions presented here show 1. that large OH fluctuations inferred by atmospheric inversions of MCF data are not due to methodological limitations made in previous studies about meteorology, type of transport model, or number of stations, and 2. that it is possible to explain MCF cycle with largely reduced OH variations when allowing MCF sources to vary within inventory bounds. Thus, a more robust determination of the magnitude of OH variations can only be attained if the uncertainties on inventories are significantly reduced, particularly when MCF variations are large in the atmosphere (e.g. late 1980s). Otherwise, MCF inversions can only provide a range of OH variations that are compatible with MCF inventory. In the other hand, the phase of OH fluctuations is more robustly determined by inversions than their amplitude. Finally, this study showed the importance to optimize simultaneously all components of a trace gas cycle.

One logical step forward to better constrain regional emission inventories is to use high frequency atmospheric observations of MCF. At stations located downwind from the main source regions, such as Mace-Head for Western Europe, synoptic changes in MCF and pollutants directly relate to their regional sources (Biraud et al., 2000, 2002). Assimilating such high-frequency data in inversions however hinges on the quality of the transport and chemistry model on short space and time scales, especially for the mixing within the planetary boundary layer. Such quality has clearly to be improved in present-day global transport models. Further, this method would require a larger number of regional source regions (up to the model grid) to be optimized (Kaminski et al., 2001; Rodenbeck et al., 2003; Peylin et al., 2005) for avoiding aggregation errors. A natural improvement of this work would be to solve MCF emissions and OH sink at the model resolution and to set up, at the same time, error correlations based on emission models and measurements. It would limit the aggregation error discussed in Sect. 3.7. This will surely require the adjoint of the CTM both for transport and chemistry, and theoretical developments to estimate possible error correlations in OH fields and MCF emissions.

The iterative method described in this work to infer inter-annual sources and sinks can be applied to any atmospheric species for which OH is the major sink as long as its lifetime is much larger than one month. This work is to be considered as a first step before applying the methodology to other atmospheric trace gas, such as methane or CFCs. Linearizing chemistry has the advantage of being able to quantify separately the effects of sources and sinks. Prescribing the range of OH variations inferred in this work in a methane inversion for instance could help optimizing inter-annual methane sources. If lifetime of the species is on the order of a few months, the method could still be used if the frequency of response functions is increased accordingly. The example of CO might be interesting to study in a near future. For short-time very active species, non-linearities might prevent from using such a linearized approach.

Appendix A

Iteration 1 of inverse procedure – application to MCF

The first iteration of the methodology described in this work requires a first-guess of inter-annual 3-D field of MCF in the atmosphere, $\hat{C}_{\mathbf{x},t}$ (Eq. 4). A natural way to calculate $\hat{C}_{\mathbf{x},t}$ is to perform an inter-annual simulation of MCF over the 1979–2000 period with LMDZ-INCA model using prior intrer-annual MCF emissions from inventory (McCulloch and Midgley, 2001) and a seasonal OH field approximately scaled to have a correct lifetime for MCF in the atmosphere (around 5 years). In the case of MCF, this is possible because estimations of inter-annual emissions are given with rather small uncertainties by inventory. For other tracers, such as methane and carbon monoxide, IAV of sources is largely unknown and can hardly be inferred using forward modeling only. Recent works have produced inter-annual simulations for CO using satellite data assimilation in CTM (Van der Werf et al., 2003; Petron et al., 2004). So it can be a problem to have a realistic first estimate of $\hat{C}_{\mathbf{x},t}$. We propose

here a methodology to produce a low-cost inter-annual simulation of a chemically active tracer, based on a linearisation of the problem, few parametrisations to extrapolate response functions in time, and a first inversion. The methodology is presented for MCF but it can be applied to other species.

The principle of the methodology is to do the calculation of $\hat{C}_{\mathbf{x},t}$ and of response functions for one reference year and then to extrapolate them to the whole 1979–2000 period in order to perform a first inversion achieving the first iteration. Doing so, calculation of inter-annual chemical response functions, the numerically expensive step of the iterative procedure, is skipped for the first iteration.

LMDZ-INCA was run to equilibrium to produce an MCF field $\hat{C}_{REF,\mathbf{x},t}$ fitting reasonably atmospheric concentrations for one year (1998 in our case). Using $\hat{C}_{REF,\mathbf{x},t}$, monthly chemical response functions are calculated for the reference year according to Eq. (5.2), with 12 months of propagation. Source response functions were calculated for the same reference year. Then, response functions had to be extended to other years from 1979 to 2000. For source response function, IAV of transport was neglected and source response function calculated for 1998 is used for all years. For OH response function, let us consider the OH sink Q due to one OH region j for month m:

$$Q_{j,m} = -k_{j,m}\,[\mathrm{OH}]_{j,m}\,C_{j,m} \tag{A1}$$

and, after differentiation:

$$\Delta Q_{j,m} = \frac{\partial Q_{j,m}}{\partial\,[\mathrm{OH}]_{j,m}}\Delta\,[\mathrm{OH}]_{j,m} + \frac{\partial Q_{j,m}}{\partial C_{j,m}}\Delta C_{j,m} \tag{A2}$$

The two terms of the sum are, respectively, the contribution of changing OH and changing MCF to the OH sink (Q). $\Delta\,[\mathrm{OH}]_{j,m}$ and $\Delta C_{j,m}$ represent the monthly changes in OH and MCF concentrations. As MCF has known large variations from 1979 to 2000, second term of Eq. (A2) cannot be neglected as in Houweling et al. (1999) for methane optimizations. So it is not possible to use the same OH response functions for the whole period. This term has to be estimated to properly represent amplitudes of OH response functions for each year. We propose here a parametrisation of the second term of Eq. (A2) as:

$$\frac{\partial Q_{j,m}}{\partial\,[\mathrm{CH_3CCl_3}]_{j,m}}\Delta\,[\mathrm{CH_3CCl_3}]_{j,m} = \frac{\partial Q_{j,m}}{\partial\,[\mathrm{OH}]_{j,m}}\Delta\,[\mathrm{OH}]_{j,m} \left(\frac{\bar{c}_{\mathrm{obs},m} - \bar{c}_{\mathrm{mod},m}}{\bar{c}_{\mathrm{mod},m}}\right), \tag{A3}$$

where $\bar{c}_{obs,m}$ and $\bar{c}_{\mathrm{mod},m}$ are, respectively, the mean observed MCF concentrations for month m at the available stations and the mean concentration of MCF in the reference simulation (1998) for month m and at the same stations. Then Eq. (A2) can be written:

$$\Delta Q_{j,m} = \frac{\partial Q_{j,m}}{\partial\,[\mathrm{OH}]_{j,m}}\Delta\,[\mathrm{OH}]_{j,m}\left(\frac{\bar{c}_{\mathrm{obs},m}}{\bar{c}_{\mathrm{mod},m}}\right) \tag{A4}$$

Relation (A4) gives an estimation of OH response function for all months m of the 1979–2000 period using the corresponding OH response function of the reference year for month m, scaled by the ratio $\frac{\bar{c}_{\mathrm{obs},m}}{\bar{c}_{\mathrm{mod},m}}$. The underlined hypothesis we make here is that the reference run of the model reproduces reasonably well the spatial and seasonal gradients of MCF in the atmosphere. We also neglected impact of varying meteorology in this extension.

Finally, response functions for stratospheric loss was treated the same way, but on a yearly basis: one yearly response function is calculated with 10 years of propagation, according to the longer timescale of this process. Then, we included stratospheric loss in the inversion after scaling the response function the same way as for OH response functions.

Using all these estimated inter-annual response functions, we performed a first inversion inferring monthly OH and MCF emissions for the period 1979–2000, followed by an inter-annual forward run with LMDZ-INCA model in which we prescribed optimized OH and optimized MCF emissions, and obtained $\hat{C}_{\mathbf{x},t}$ that has been used for the second iteration.

Appendix B

Inverse formulation (see Bousquet et al., 1999, 2000 and Peylin et al., 1999, 2002 for more details)

During the 1979–2000 period, we optimize scaling factors (vector α) for MCF surface sources and sinks (monthly), OH concentrations (monthly) and stratospheric loss (annually) by minimizing $J(\alpha)$ that can be written from Eq. (6):

$$J(\alpha) = \frac{1}{2}\left((\mathbf{y}_{\mathrm{obs}} - \mathbf{H}\alpha)^T\,\mathbf{R}^{-1}\,(\mathbf{y}_{\mathrm{obs}} - \mathbf{H}\alpha) + (\alpha - \alpha_b)^T\,\mathbf{P}^{-1}\,(\alpha - \alpha_b)\right),$$

where $\mathbf{R}$ is the variance-covariance matrix of error of observations, $\mathbf{P}$ is the variance-covariance matrix of error of state vector α, α_b is a prior estimate of α, $\mathbf{y}_{\mathrm{obs}}$ is the vector of observations and $\mathbf{H}$ is the Jacobian matrix of response functions $\tilde{C}$. The first term of J relies to the weighted distances between model and measurements and the second term to weighted distance between variables and their prior estimate. The second term of J is a Bayesian regularization term (Tarantola et al., 1987). We suppose that errors are uncorrelated and follow a normal probabilistic law. The value α_a of the state vector α at the minimum of J and its variance/covariance matrix are given by (Tarantola, 1987):

$$\alpha_a = \alpha_b + \left(\mathbf{H}^T\mathbf{R}^{-1}\mathbf{H} + \mathbf{P}^{-1}\right)^{-1}\mathbf{H}^T\mathbf{R}^{-1}\,(y_{\mathrm{obs}} - \mathbf{H}\alpha_b)$$

$$\mathbf{P}_a = \left(\mathbf{H}^T\mathbf{R}^{-1}\mathbf{H} + \mathbf{P}^{-1}\right)^{-1}$$

Table A1. Contribution of changing MCF and of changing OH to OH sink variations. See text for details.

	$\bar{C}$ ppt	$[\bar{OH}]\times10^5$ cm^{-3}	$\frac{\Delta\bar{C}}{\Delta t}$ ppt.yr^{-1}	$\frac{\Delta[OH]}{\Delta t}\times10^5$ cm^{-3}.yr^{-1}	$\bar{C}\times\frac{\Delta[OH]}{\Delta t}$	$[\bar{OH}]\times\frac{\Delta\bar{C}}{\Delta t}$
1980–1989	100	10.1	+4.5	+0.01	+1	+45
1985–1995	100	9.9	−7.5	−0.07	−7	−75
1990–2000	85	9.5	−9.1	−0.1	−8.5	−86

Appendix C

Extrapolation of response functions after propagation time

Inter-annual source and chemical response functions were treated separately after linearising the mass conservation equation (Eq. 5). They were all propagated for 6 months in time. Thus an extrapolation was necessary to use them in the inverse procedure. For source response functions, we completed the 6 months with a 1-year response function calculated using 1998 meteorology only (1st iteration) and then extrapolated it towards the asymptotic value at the end of the period of inversion. The asymptotic value is given by the limit concentration of MCF in ppt reached after an infinite dilution of 1 Gg of MCF in the atmosphere. It is equal to 0.042 ppt/Gg. because, as sources and sinks are solved separately, MCF pulse sources are treated as if MCF was a passive tracer.

Chemical response functions were completed by exponential extrapolation towards the asymptotic value. The asymptotic value is known because after one month (one year for photolysis) of chemical removal, the total mass of MCF remains constant, being just diluted by atmospheric transport. We calculated this amount and compute the global mean concentration of MCF that should be reached if run was performed indefinitely. Symmetrically to MCF source pulses, no MCF sources are prescribed while solving for chemical sinks, as sources and sinks are solved separately (Eq. 5).

Appendix D

Curve fitting method (see Thoning et al., 1989 for details)

We apply the curve fitting method of Thoning et al. (1989) to atmospheric data of MCF. We fitted a function to observations defined as a second-order polynomial plus three harmonics to account for eventual seasonal variations. Residuals are defined as the differences between observed monthly means and function. Residuals were filtered using a loess smoother with a span of 2 years to remove high frequency and seasonal variations. Trend (in ppt) was calculated as the sum of the second-order polynomial and filtered residuals. Trend reveals the long-term evolution of MCF in the atmosphere. Growth rate (in ppt.yr^{-1}) was calculated as the first derivative of the trend. In several studies (KR and PR) the word "trend" is used instead of growth rate.

Appendix E

Estimation of long-term evolution of OH sink

Observed MCF growth rate is due to emissions and transport of MCF from one part and removal by OH and by photolysis from another. OH sink (Q) can be decomposed into two terms following Eq. (2):

$$Q = -k\,[\mathrm{OH}]\,C \tag{A5}$$

Long term trend of OH sink ($\overline{\frac{\Delta Q}{\Delta t}}$) can be written, after extracting long-term trend of OH and C:

$$\overline{\frac{\Delta Q}{\Delta t}} = -k\left[\bar{C}\,\overline{\frac{\Delta\,[\mathrm{OH}]}{\Delta t}} + \overline{[\mathrm{OH}]}\,\overline{\frac{\Delta C}{\Delta t}}\right] \tag{A6}$$

Table A1 gives typical order of magnitudes of the two terms in brackets for following decades: 1980s, 1985–1995 and 1990–2000. $\overline{C}$ is evaluated using ALE/GAGE/AGAGE stations, $\overline{[OH]}$ is taken from Table 1, $\overline{\frac{\Delta[OH]}{\Delta t}}$ is the OH trend calculated from the results of Sect. 3 (+0.1% in the 1980s, −0.7%.yr^{-1} for 1985–1995 and −1.0%.yr^{-1} for 1990–2000), and long-term trend of MCF concentration ($\overline{\frac{\Delta C}{\Delta t}}$) is evaluated using observed growth rate of Fig. 11. In all periods, the long-term contribution of changing OH is not larger than 10% of the contribution of changing MCF. This is due to large variations of MCF emissions (on a decadal basis) between the 1980s and the 2000s. If we use the OH trend of the ±15% error case, the difference is even larger because OH variability is reduced. In other words, a small error in the calculation of prior OH sink could significantly modify OH trend. Possible causes of errors are transport processes, spatial patterns of OH field (prescribed monthly in this work), rates of reaction with OH, rate of photolysis in the stratosphere, underestimated error on the sources,... Another final remark is that such a small atmospheric contribution due to OH trend (maximum of few ppt/yr) is on the order of observation error, which also limits the consistency of small OH trends inferred by inversions. However, as for year-to-year variations, phasing of OH trend seems more robust than its amplitude.

Acknowledgements. We kindly thank all scientists and technicians from ALE/GAGE/AGAGE and from NOAA/CMDL for their effort to collect and analyze atmospheric samples all over the world. We especially thank the R. G. Prinn and S. A. Montzka to make data of their respective group available at WMO Web site. We thank M. Krol for stimulating discussions and comments on this work. French atomic agency (CEA) and its computing center (CCRT) are to be thanked for the large computational support they gave to this project. We thank A. Faure for statistical expertise.

Edited by: M. Heimann

References

Biraud, S., Ciais, P., Ramonet, M., Simmonds, P., Kazan, V., Monfray, P., O'Doherty, S., Spain, T. G., and Jennings, S. G.: European greenhouse gas emissions estimated from continuous atmospheric measurements and radon 222 at Mace Head, Ireland, J. Geophys. Res.-A, 105 (D1), 1351–1366, 2000.

Biraud, S., Ciais, P., Ramonet, M., Simmonds, P., Kazan, V., Monfray, P., O'Doherty, S., Spain, G., and Jennings, S. G.: Quantification of carbon dioxide, methane, nitrous oxide and chloroform emissions over Ireland from atmospheric observations at Mace Head, Tellus Series B – Chemical and Physical Meteorology, 54 (1), 41–60, 2002.

Bousquet, P., Ciais, P., Peylin, P., Ramonet, M., and Monfray, P.: Inverse modeling of annual atmospheric CO2 sources and sinks 1. Method and control inversion, J. Geophys. Res.-A, 104 (D21), 26 161–26 178, 1999.

Bousquet, P., Peylin, P., Ciais, P., Le Quere, C., Friedlingstein, P., and Tans, P. P.: Regional changes in carbon dioxide fluxes of land and oceans since 1980, Science, 290 (5495), 1342–1346, 2000.

Brenninkmeier, C. A. M., Manning, M. R., Lowe, D. C., Wallace, G., Sparks, R. J., and Volz-Thomas, A.: Interhemispheric asymmetry in OH abundance inferred from meazsurements of atmospheric CO_2, Nature, 356, 50–52, 1992.

Dentener, F., Peters, W., Krol, M., van Weele, M., Bergamaschi, P., and Lelieveld, J.: Inter-annual variability and trend of CH4 lifetime as a measure for OH changes in the 1979–1993 time period, J. Geophys. Res.-A, 108 (D15), 4442, doi:10.1029/2002JD002916, 2003.

Dlugokencky, E. J., Houweling, S., Bruhwiler, L., Masarie, K. A., Lang, P. M., Miller, J. B., and Tans, P. P.: Atmospheric methane levels off: Temporary pause or a new steady-state?, Geophys. Res. Lett., 30 (19), 1992, doi:10.1029/2003GL018126, 2003.

Engelen, R. J., Denning, A. S., Gurney, K. R., and TRANSCOM modelers: On error estimation in atmospheric CO_2 inversions, J. Geophys. Res.-A, 107, ISI:000180867500041, 2002.

Enting, I. G. and CSIRO: Division of Atmospheric Research, Synthesis inversion of atmospheric CO2 using the GISS tracer transport model, CSIRO Division of Atmospheric Research technical paper; Aspendale, Vic.: CSIRO, Division of Atmospheric Research, 29, 44, 1993,

Gerbig, C., Lin, J. C., Wofsy, S. C., Daube, B. C., Andrews, A. E., Stephens, B. B., Bakwin, P. S., and Grainger, C. A.: Toward constraining regional-scale fluxes of CO_2 with atmospheric observations over a continent: 2. Analysis of COBRA data using a receptor-oriented framework, J. Geophys. Res.-A, 108 (D24), 4757, doi:10.1029/2003JD003770, 2003.

Hauglustaine, D. A., Brasseur, G. P., Walters, S., Rasch, P. J., Muller, J. F., Emmons, L. K., and Carroll, C. A.: MOZART, a global chemical transport model for ozone and related chemical tracers 2. Model results and evaluation, J. Geophys. Res.-A, 103 (D21), 28 291–28 335, 1998.

Hauglustaine, D. A., Hourdin, F., Jourdain, L., Filiberti, M. A., Walters, S., Lamarque, J. F., and Holland, E. A.: Interactive chemistry in the Laboratoire de Meteorologie Dynamique general circulation model: Description and background tropospheric chemistry evaluation, J. Geophys. Res.-A, 109 (D4), 3414, doi:10.1029/2003JD003957, 2004.

Holton, J. R.: An introduction to dynamic meteorology, International series, Academic press, 1979.

Hourdin, F.: On the use of finite volume methods for atmospheric advection of trace species: I. Test of various formulations in a General Circulation Model, Monthly Weather Review, 127, 822–837, 1999.

Hourdin, F. D., Couvreux, F., and Menut, L.: Parameterization of the dry convective boundary layer based on a mass flux representation of thermals, J. Atmos. Sci., 59 (6), 1105–1123, 2002.

Houweling, S., Dentener, F., Lelieveld, J., Walter, B., and Dlugokencky, E.: The modeling of tropospheric methane: How well can point measurements be reproduced by a global model?, J. Geophys. Res.-A, 105 (D7), 8981–9002, 2000.

Houweling, S., Kaminski, T., Dentener, F., Lelieveld, J., and Heimann, M.: Inverse modelling of methane sources and sinks using the adjoint of a global transport model, J. Atmos. Res., 104, 26 137–26 160, 1999.

IPCC: Climate change 2001, The science of climate change, Change 2001, Cambridge University Press, 2001.

Kaminski, T., Rayner, P. J., Heimann, M., and Enting, I. G.: On aggregation errors in atmospheric transport inversions, J. Geophys. Res.-A, 106 (D5), 4703–4715, 2001.

Krol, M. C., Lelieveld, J., Oram, D. E., Sturrock, G. A., Penkett, S. A., Brenninkmeijer, C. A. M., Gros, V., Williams, J., and Scheeren, H. A.: Continuing emissions of methyl chloroform from Europe, Nature, 421 (6919), 131–135, 2003.

Krol, M. and Lelieveld, J.: Can the variability in tropospheric OH be deduced from measurements of 1,1,1-trichloroethane (methyl chloroform)?, J. Geophys. Res.-A, 108 (D3), 4125, doi:10.1029/2002JD002423, 2003.

Law, R. M., Rayner, P. J., Denning, A. S., Erickson, D., Fung, I. Y., Heimann, M., Piper, S. C., Ramonet, M., Taguchi, S., Taylor, J. A., Trudinger, C. M., and Watterson, I. G.: Variations in modeled atmospheric transport of carbon dioxide and the consequences for CO2 inversions, Global Biogeochem. Cycles, 10 (4), 783–796, 1996.

Lawrence, M. G., Jockel, P., and von Kuhlmann, R.: What does the global mean OH concentration tell us?, Atmos. Chem. Phys., 1, 37–49, 2001,
SRef-ID: 1680-7324/acp/2001-1-37.

Lelieveld, J., Peters, W., Dentener, F. J., and Krol, M. C.: Stability of tropospheric hydroxyl chemistry, J. Geophys. Res.-A, 107 (D23), 4712-ACL1, doi:10.1029/2002JD002272, 2002.

McCulloch, A. and Midgley, P. M.: The history of methyl chloroform emissions: 1951–2000, Atmos. Environ., 35 (31), 5311–5319, 2001.

Millet, D. B. and Goldstein, A. H.: Evidence of continuing methylchloroform emissions from the United States, Geophys.

Res. Lett., 31, 4026, doi:10.1029/2004GL020166, 2004.

Montzka, S. A., Spivakovsky, C. M., Butler, J. H., Elkins, J. W., Lock, L. T., and Mondeel, D. J.: New observational constraints for atmospheric hydroxyl on global and hemispheric scales, Science, 288 (5465), 500–503, 2000.

NCI: Le cycle mondial de l'industrie électronique, in: Note de conjoncture internationale, Direction de la prévision et de l'analyse économique, Editor. March 2003, Ministère de l'économie, des finances et de l'industrie: Paris, France (http://www.finances.gouv.fr/Prevision/nci/nci0303/nci0303.htm), 2003.

Olivier, J. G. J. and Berdowski, J. J. M.: Global emissions sources and sinks, in: The Climate System, edited by: Berdowski, J., Guicherit, R., and Heij, B. J., A. A. Balkema Publishers/Swets & Zeitlinger Publishers, Lisse, The Netherlands, ISBN 90 5809 255 0, 33–78, 2001.

Peylin, P., Bousquet, P., Ciais, P., and Monfray, P.: Time-Dependant vs Time-Independant inversion of the atmospheric CO_2 observations: consequences for the regional fluxes, in: Inverse methods in global biogeochemical cycles, Geophysical Monograph 114, edited by: Kashibata, P., Heimann, M., Rayner, P., Mahowald, N., Prinn, R. G., and Hartley, D. E., American Geophysical Union, Washington, D.C., 1999.

Peylin, P., Rayner, P. J., Bousquet, P., Carouge, C., Hourdin, F., Heinrich, P., Ciais, P., and AEROCARB contributors: Daily CO_2 flux estimate over Europe from continuous atmospheric measurements: part 1 inverse methodology, Atmos. Chem. Phys. Discuss., 5, 1647–1678, 2005,
SRef-ID: 1680-7375/acpd/2005-5-1647.

Prinn, R. G., Weiss, R. F., Miller, B. R., Huang, J., Alyea, F. N., Cunnold, D. M., Fraser, P. J., Hartley, D. E., and Simmonds, P. G.: Atmospheric Trends and Lifetime of Ch3ccl3 and Global Oh Concentrations, Science, 269 (5221), 187–192, 1995.

Prinn, R. G., Weiss, R. F., Fraser, P. J., Simmonds, P. G., Cunnold, D. M., Alyea, F. N., O'Doherty, S., Salameh, P., Miller, B. R., Huang, J., Wang, R. H. J., Hartley, D. E., Harth, C., Steele, L. P., Sturrock, G., Midgley, P. M., and McCulloch, A.: A history of chemically and radiatively important gases in air deduced from ALE/GAGE/AGAGE, J. Geophys. Res.-A, 105, 17 751–17 792, 2000.

Prinn, R. G., Huang, J., Weiss, R. F., Cunnold, D. M., Fraser, P. J., Simmonds, P. G., McCulloch, A., Harth, C., Salameh, P., O'Doherty, S., Wang, R. H. J., Porter, L., and Miller, B. R.: Evidence for substantial variations of atmospheric hydroxyl radicals in the past two decades (Vol. 292, p. 1882, 2001), Science, 293 (5532), 1048–1048, 2001.

Rayner, P. J. and Law, R. M.: A comparison of modelled responses to prescribed CO_2 sources, CSIRO, Aust. Atmos. Res. Tech. Pap., 1995.

Reimann, S., Manning, A. J., Simmonds, P. G., Cunnold, D. M., Wang, R. H. J., Li, J. L., McCulloch, A., Prinn, R. G., Huang, J., Weiss, R. F., Fraser, P. J., O'Doherty, S., Greally, B. R., Stemmler, K., Hill, M., and Folini, D.: Low European methyl chloroform emissions inferred from long-term atmospheric measurements, Nature, 433(7025), 506–508, 2005.

Tarantola, A.: Inverse problem theory, Elsevier, Amsterdam, The Netherlands, 1987.

Thoning, K. W., Tans, P. P., and Komhyr, W. D.: Atmospheric carbon dioxide at Mauna Loa Observatory, 2. Analysis of the NOAA GMCC data, 1974, 1985, J. Geophys. Res., 94 (D6), 8549–8565, 1989.

Tiedtke, M.: A comprehensive flux scheme for cumulus parametrization inlarge-scale models, Monthly Weather Review, 117, 1779–1800, 1989.

Wang, J. S., Logan, J. A., McElroy, M. B., Duncan, B. N., Megretskaia, I. A., and Yantosca, R. M.: A 3-D model analysis of the slowdown and inter-annual variability in the methane growth rate from 1988 to 1997, Global Biogeochem. Cycles, 18 (3), 3011, doi:10.1029/2003GB002180, 2004.

Warwick, N. J., Bekki, S., Law, K. S., Nisbet, E. G., and Pyle, J. A.: The impact of meteorology on the inter-annual growth rate of atmospheric methane, Geophys. Res. Lett., 29 (20), 1947, doi:10.1029/2002GL015282, 2002.

Wennberg, P. O., Peacock, S., Randerson, J. T., and Bleck, R.: Recent changes in the air-sea gas exchange of methyl chloroform, Geophys. Res. Lett., 31 (16), 112, doi:10.1029/2004GL020476, 2004.

WMO (World Meteorological Organization): Scientific Assessment of Ozone Depletion, 498, 2002.

Yvon-Lewis, S. A. and Butler, J.: Effect of oceanic uptake on atmospheric lifetimes of selected trace gases, J. Geophys. Res.-A, 107, doi:10.1029/2001JD001267, 2002.